EFFECTS OF UPSTREAM ENERGY SAVING DEVICES ON ENGINE OPERATION

N.S. SHARMA

TU Delft

EFFECTS OF UPSTREAM ENERGY SAVING DEVICES ON ENGINE OPERATION

Nikhil S Sharma

August 16, 2019

SDPO.19.022.m

to obtain the degree of Master of Science in Marine Technology at the Delft University of Technology

to be defended publicly on Tuesday August 27^{th}, 2019 at 10:00 AM

Thesis committee:

Ir. K. Visser
assistant professor of Marine Engineering
Dr. ir. P. de Vos
assistant professor of Marine Engineering
Dr. ir. H.J. de Koning Gans
assistant professor of Ship Hydromechanics

Supervisors:

Ir. K. Visser
assistant professor of Marine Engineering
Dr. ir. P. de Vos
assistant professor of Marine Engineering

Faculty of Mechanical, Maritime and Materials Engineering
Marine and Transport Technology
Design, Production and Operation

TU Delft Delft University of Technology

Abstract

Rising carbon emissions and International Maritime Organisation (IMO) have put immense pressure on ship owners to make ships more efficient. One way to make ships more efficient is to install an energy saving device (ESD). ESDs are designed to perform at vessel's design speed and design draft. Thus, there is abundant information available on how they perform at the design speed or speeds close to it. However, their performance in part-load conditions remains a question mark. Although, these devices are used for ships having a high block coefficient and ships that sail at their design speed or close to it for the most part of their voyage, it is still important to assess their performance in part-load conditions and how they affect the engine operation.

The purpose of this thesis is to shed some light on the performance of three upstream ESDs on engine operation particularly, in part-load conditions. These three devices are Pre-duct, Pre-swirl stator and Mewis duct. Model tests and CFD self propulsion simulations are used to assess their performance before implementing them. ESDs have been present since the first half of the 20th century. But despite that, their assumed working principle is still debatable. Performing simulations at all ship speeds is complex and time consuming. Hence, a new approach is proposed in this graduation report wherein a linear approach towards increase/decrease in specific propeller losses, influenced by the ESD, with respect to advance coefficient J is postulated. Advance coefficient is a dimensionless term defined as the ratio of the velocity of advance i.e the speed at which the water passes through the propeller disc, to the product of rotation rate and diameter of the propeller. The influence on losses is case dependent i.e depends on the type of ESD installed. The propeller is associated with three kinds of losses : axial, rotational and frictional losses. ESDs influence one or more of these losses to increase the propulsive efficiency. Therefore, the energy saving effect of these upstream ESDs increases linearly with advance coefficient. This new approach sheds some light on the performance of upstream ESDs i.e devices installed before the propeller, in part load conditions and helps in predicting their performance in low-medium speed range. This postulation is then implemented on a propeller loss diagram to make a simplistic model. This model is then implemented on the engine of a chemical tanker to assess the performance of the aforementioned ESDs.

The effect of these devices on engine operation is discussed and the model yields power savings for all the ESDs at design speed and speeds to close to it. However, it is found that power savings are marginal in part-load conditions even though the gain in propulsive efficiency is more or less the same at all speeds. This raises the question whether power savings in part-load condition even matter. A reduction in Energy Efficiency Design Index (EEDI) is also seen for the three ESDs. It is recommended to further study the postulation that the decrease or increase in losses associated with the propeller, influenced by these ESDs, varies linearly with advance coefficient.

Preface

The last two years were quite challenging but also a wonderful part of my life. I made a lot of friends and learned a lot, not only about the marine technology courses but also about professionalism in general. I used to sail as an engineer on bulk carriers before I started my masters at the TU Delft. Having already worked on-board a vessel, I thought I knew almost everything there is to know about the shipping industry. However, I was taken completely by surprise when I started attending the lectures at the university. I realised I had so much to learn and TU Delft was the perfect place for this. My interest in energy saving devices developed after attending the course of marine propulsion systems in last quarter of my first year at the university.

I am very grateful to my supervisors, Ir. Klaas Visser and Dr. ir. Peter de Vos for helping, guiding and keeping me on track in these past nine months. I would also like to thank Prof Dr. ir. Tom van Terwisga for helping me understand the working principle of energy saving devices.
I'd like to thank my friends who have shown great support in these two years. I'd also like to thank the external committee member, Dr. ir. H.J. Koning Gans, for taking time out of his busy schedule and attending and grading my graduation.
Last but not the least, I am immensely grateful to my parents and my brother for supporting me not only during my master's but throughout my life. It would not have been possible without you three.

List of Figures

List of Tables

List of symbols

J	Advance coefficient	$[-]$
ϕ_{mx}	Momentum flux	$[kg/sm]$
R_{bh}	Resistance of bare hull	$[kgm/s^2]$
ρ	Density of water	$[kg/m^3]$
u_x	component of velocity in axial direction	$[m/s]$
U_0	Ship speed	$[m/s]$
n_x	normal vector in x-direction	$[-]$
T	Propeller thrust	$[kgm/s^2]$
t	Thrust deduction factor	$[-]$
P	Power	$[kgm^2/s^3]$
C_T	Propeller thrust loading coefficient	$[-]$
A_p	Propeller disc area	$[m^2]$
p, p_0	Pressure	$[kg/ms^2]$
ψ	Viscous Dissipation	$[kgm^2/s^2]$
u_r	Radial velocity	$[m/s]$
u_ϕ	Tangential velocity	$[m/s]$
Q	Propeller Torque	$[kgm^2/s^2]$

K_Q	Torque coefficient	$[-]$
K_T	Thrust coefficient	$[-]$
η_D	Propulsive efficiency	$[-]$
η_o	Open water efficiency	$[-]$
η_h	Hull efficiency	$[-]$
η_R	Relative rotative efficiency	$[-]$
n	Rotation rate	$[1/s]$
V_s	Ship speed	$[m/s]$
D	Propeller diameter	$[m]$
η_{WP}	Blade loading efficiency	$[-]$
$\eta_{T/Q}$	Blade efficiency	$[-]$
η_{INT}	Interaction efficiency	$[-]$
α	Angle of attack	$[°]$
β_P	pitch angle	$[°]$
β	Hydrodynamic pitch angle	$[°]$
V_x	Velocity of advance	$[m/s]$
V_T	Tangential velocity	$[m/s]$
η_a	Axial efficiency	$[-]$
η_r	Rotational efficiency	$[-]$
η_f	Frictional efficiency	$[-]$
f_{esd}	Energy saving factor	$[-]$
η_{o+}	Efficiency with +2% deviation from average gain	$[-]$
η_{o-}	Efficiency with -2% deviation from average gain	$[-]$
L_{PP}	Length between perpendiculars	$[m]$
B	Breadth	$[m]$
H	Depth	$[m]$
T	Design draft	$[m]$
Δ	Displacement	$[m]$
C_E	Specific resistance	$[-]$
w	Wake fraction	$[-]$
P_E	Effective towing power	$[kgm^2/s^3]$
P_S	Shaft power	$[kgm^2/s^3]$
P_D	Delivered power	$[kgm^2/s^3]$
P_B	Brake power	$[kgm^2/s^3]$
η_{TRM}	Transmission efficiency	$[-]$
C	Fuel to CO_2 conversion factor	$[-]$

f_c	Correction factor for capacity	[−]
f_w	Correction factor for performance in real weather	[−]
f_i	Correction factor for efficiency	[−]

List of abbreviations

IMO	International Maritime Organisation
ESD	Energy Saving Device
CFD	Computational Fluid Dynamics
EEDI	Energy Efficiency Design Index
MIDP	Mitsui Integrated Duct
HZN	Hitachi Zosen Nozzle
WED	Wake Equalizing Duct
SILD	Sumitomo Integrated Lammeren Duct
SDS-F	Semi-Duct System with contra-Fins
CPP	Controllable pitch propeller
BSD	Blade Efficiency Improving Duct
AXL	Axial losses
ROTL	Rotational losses
VISL	Viscous losses
GHG	Green House Gas
CO_2	Carbon Dioxide
UN	United Nations
LNG	Liquefied Natural Gas
HFO	Heavy Fuel Oil
TEU	Twenty Foot Equivalent
PBCF	Propeller Boss Cap with Fins
GRIP	Green Retrofitting through Improved Propulsion

Contents

1 Introduction

1.1 Background

Energy saving devices (ESDs) have been present since the first half of the 20^{th} century. One of the first papers to be published was about a nozzle in front of a propeller to increase the fuel efficiency by van Lammeren in 1949. Since then, various research papers have been published over the years, introducing new ESDs, their working principle and their benefits. Work on these devices started gaining momentum during the seventies because of the oil crisis. Numerous devices were investigated and most of them were rejected due to structural failure, lack of accuracy in full-scale measuring capability, lack of transparency of the savings in actual operating conditions and limited insight into the working principles of the devices [1]. Energy saving ranging from 2-8% is claimed by manufacturers and although these devices have been commercially successful, their working principle hasn't been fully understood. Terwisga et al.[2] give a brief overview of these devices in their research paper. The evolution of upstream ESDs over the years can be seen in figure 1.

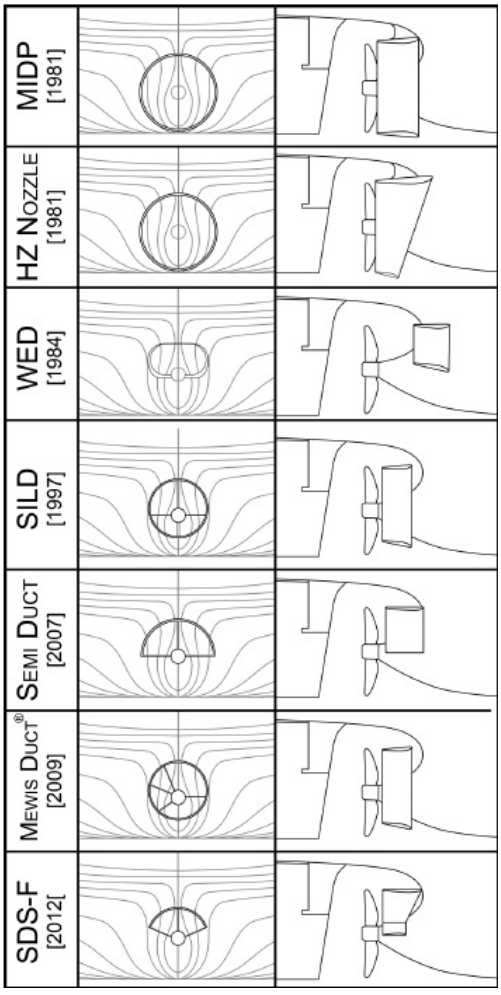

Figure 1: Evolution of upstream ducted ESDs[2]

The Mitsui Integrated Duct (MIDP) is the first commercial ESD. It is an annular steel nozzle located immediately in front of the propeller and slightly asymmetric about its axis. The Hitachi Zosen Nozzle (HZN) was developed in the same year as MIDP and is similar to MIDP with the exception of being more non-axisymmetric. One of the most popular ESDs is probably the Wake Equalizng Duct (WED) developed by Schneekluth. It consists of two half rings ducts installed in front of the propeller. The Sumitomo Integrated

Lammeren Duct (SILD) is geometrically similar to the MIDP and the Becker Mewis is similar to the SILD. The only difference between these three ESDs was how they are mounted in the front of the propeller. Kawaki's Semi-Duct System with contra-Fins (SDS-F), unlike the Becker Mewis Duct, used a semi-circular duct instead of fully circular ducts[2]. Despite the existence of the ESDs for so many decades, the working principles of these devices is still an ongoing debate. Another debatable topic of discussion regarding ESDs are the scaling procedures used in model testing to predict full-scale performance. This difficulty comes from the Reynolds number effects such as separation which occurs on the model, may not occur at full scale and the boundary layer thickness is also likely to be different at full scale[3]. Abundant information is available on the performance of these devices at design speed and speeds close to it, however, there isn't any information available on how these devices would perform at low-medium ship speeds or on their effect on the engine in part-load conditions.

1.2 Objective

The purpose of this master's thesis is to predict the performance of three upstream ESDs - Pre-duct, Pre-swirl stator, Mewis Duct in part-load conditions and their effect on the engine operation. This will be done by making a simplistic model for propeller partial efficiencies. The model will be then be used to assess the performance of the aforementioned ESDs on a chemical tanker. Here, part-load conditions indicates that the vessel is moving at low-medium speeds. Although, the tanker has a controllable pitch propeller (CPP), the performance of the aforementioned ESDs will be assessed on a constant pitch ratio of 0.7075. ESDs are designed to give maximum performance at design speed or speeds close to the design speed. However, their performance in part load conditions or low-medium speed range, remains a question mark. Model tests and CFD self propulsion simulations are used to visualize and assess their performance before implementing them. But despite that, their assumed working principle is still debatable. Terwisga et al.[2] propose a new alternative approach to understand the working principles of ESDs using a Blade efficiency improving stator duct (BSD), which is a preswirl stator for their research. This new approach also sheds some light on the performance of upstream ESDs i.e devices installed before the propeller such as pre-ducts, prewirl stators etc in part load conditions and provides the basis for a postulation to predict their performance in low-medium speed range. This postulation is then used to assess the performance of these devices on the engine of *Castillo De Tebra* and answer the main research question mentioned below.

Main Research Question
What is the effect of upstream energy saving devices on engine operation (in design and part-load conditions)?

The main research question is also answered with the help of the sub-questions mentioned below.

Sub-Questions

1. *What kind of upstream ESDs exist?*
2. *How do upstream ESDs perform in design and part-load condition?*
3. *How can the performance of ESDs in part-load condition be modelled simplistically without CFD?*
4. *What is the effect of these devices on engine operation in part-load conditions. Explain with the help of case study.*
5. *What is the effect on EEDI in part-load condition? Explain with the help of a case study.*

1.3 Scope and Methodology

Global warming is a major concern today and the need for energy saving has increased now more than ever as the rising CO_2 levels lead to global warming. In the 'Paris Agreement for Shipping' held in April 2018, the UN

International Maritime Organization (IMO) came with an ambition of reducing the CO_2 emissions per year by at least 50% by 2050, when compared to 2008. Furthermore, IMO has also set an ambitious goal of improving the efficiency by 40% by 2030 and by 70% by 2050, as long as fossil fuels are still in use[4]. In figure 2, the blue line indicates the decrease in CO_2 by 50% by 2050 and limit the global warming to 2°and the orange line indicates a decrease in CO_2 by 100% and limit the global warming to 1.5°. IMO's main motive behind EEDI was to devise an index to represent GHG (Green House Gas) emissions from. Since marine GHG emissions consists primarily of CO_2, the EEDI is representative of CO_2 emission.
There is abundant information available on ESDs on design speed as they are designed to perform at these speeds, however, there isn't any information available about their performance at low-medium speeds. This information is either confidential or just not assessed as ESDs are used on ships having a high block coefficient, which sail at their design speed or close to it most of the time. One way to assess their performance at part-load conditions would be perform CFD open water or self-propulsion simulations at all speeds. This approach, nonetheless, is not used as performing simulations at all speeds is complex and is not viable within the given time frame of this project. Therefore, an analytical approach is used to predict the performance of upstream ESDs on engine operation. This approach is described briefly in the next section 1.4. ESDs can help the existing and new ships meet the EEDI requirements of the immediate future.

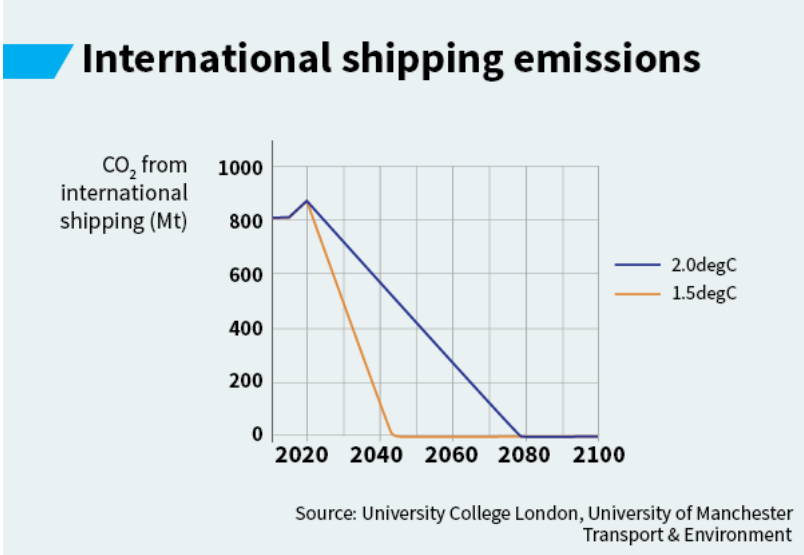

Figure 2: Shipping emissions and effect on global warming

1.4 Postulation

The postulation will focus on three upstream ESDs: Pre-duct, Preswirl stator and Mewis duct. The losses associated with the propeller are axial, rotational and frictional. This can been seen in figure 3. *It is postulated that the energy saving effect increases linearly with advance coefficient J.* J is a dimensionless term defined by the ratio of velocity of advance (velocity of water passing through the propeller disc) to the product of the rotation rate and diameter of the propeller. This energy saving effect depends on the ESD and its influence on the losses. For example, a pre-swirl stator will have a positive influence on rotational losses as J increases i.e it will decrease the rotational losses as J increases. Whereas, a pre-duct will have a negative influence on axial losses as J increases but, the overall influence will still lead to an increase in efficiency. A mewis duct is more or less a combination of a pre-swirl stator and a pre-duct and affects both axial and rotational losses. All the three upstream ESDs increase frictional losses as they lead to additional surface area. The basis for this postulation is discussed in detail in chapter 3 under section 3.1.

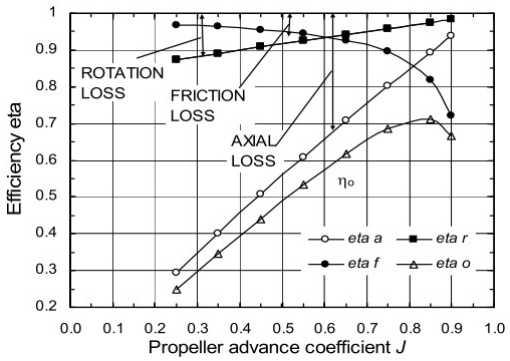

Figure 3: Losses associated with a propeller[5]

2 Literature Review

2.1 Energy saving

The primary factors influencing power consumption are the total resistance of the vessel and the propulsive efficiency determined by the propeller and its arrangement behind the hull. A new vessel design can address these aspects during the design process. However, an existing vessel does not have this option. Fuel consumption can be reduced by reducing required power for propulsion or by using alternate fuel power such as electric or solar energy or dual fuel engines.

An effective way to reduce fuel consumption is to reduce the service speed. A well known rule of thumb is that power scales with the third power of speed which basically means that a 10% speed reduction would lead to about 27% ($0.9^3 = 0.73$) power saving. Test results on a 4200 TEU (Twenty foot equivalent) container show that sailing at 24 knots instead of 25 knots reduces the power consumption by 13%. And sailing at 23 knots reduces the power demand by 26% which means that in most cases a smaller main engine with lower investment can be installed and large fuel savings in the fuel oil consumption can be gained[6]. However, slow-steaming is not always viable due to reduced transport capacity and higher crew costs. The capital cost of cargo also depends on both cargo value and transport time. According to Terwisga et al.[2], one of the ways to reduce required power, other than by reducing the ship resistance is to improve the propeller-hull interaction, hence decreasing the thrust deduction. This results in lower required thrust and consequently reduction in power required to propel the ship. Another way is to improve the efficiency of the propulsor itself. This is can be done in several ways:

1. By reorienting the total force vector acting on a propeller blade in a more favourable direction. This is to improve the thrust to torque ratio.

2. Improving the radial load distribution.

3. Reducing the hub vortex.

The efficiency of a propeller is often defined as the ratio of useful power to the delivered power. However, this definition is not very useful when two propellers need to be compared. According to Olsen [7], a better insight can be gained by comparing different energy losses associated with the propellers. Hence, the efficiency of a propeller is calculated by energy coefficients which are related to four types of losses i.e the axial, the rotational, the frictional and the finite blade number loss and one gain, which is the axial gain. In 2013, Terwisga[8] made steps towards gaining an insight into the working principles of ESDs using energy analysis.

Let's take an example of a deeply submerged axisymmetric hull in an axial flow as shown in figure 4

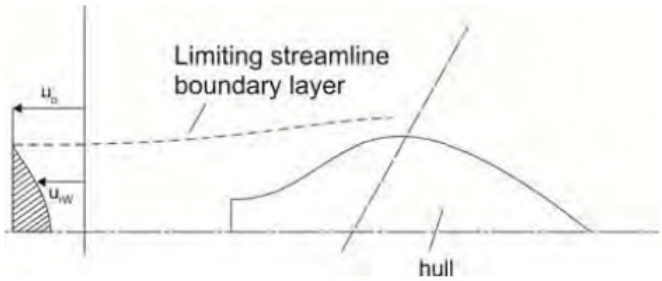

Figure 4: Velocity profile in the wake of bare hull[8]

Energy balance considerations

From Newton's second law, it can be said that the resistance force experienced by the hull due to the flow of water is represented by the change in momentum flux between the incoming, undisturbed momentum flux and the outgoing flux at the considered transverse exit plane in the wake[8].

$$\phi_{mxi} - \phi_{mxo} = R_{bh} \tag{1}$$

where $\phi_{mx} = \rho \int_{A_w} {u_x}^2 n_x dA$ and A_w is area in wake of bare hull. R_{bh} is the resistance of the bare hull and ρ is the fluid density.

When a propeller is introduced, the momentum equation can be rewritten to :

$$R_p - T = \rho \int_{A_{WP}} u_x(u_x - U_0)dA \tag{2}$$

where u_0 is the ship speed, u_x is the velocity in axial direction and T is the propeller thrust.

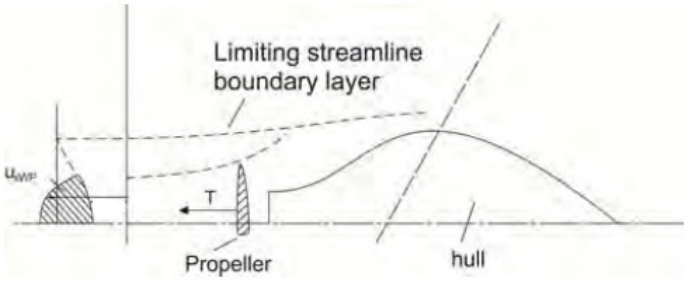

Figure 5: Velocity profile in the wake of self propelled hull[8]

The resistance of the hull in the self propelled condition is different from the resistance of the bare hull[8].

$$T(1 - t) = R_{bh} \tag{3}$$

where this difference is accounted for by a thrust deduction factor t.
Terwisga[8] concludes that for a steady state condition, there isn't a net contribution to the change in momentum flux between in and outflow plane. Therefore, all effects of ESDs must appear through an effect in the energy losses in the flow.

As mentioned section 2.1, an alternative way of determining the efficiency of the propeller is by analysing the losses associated with the propeller:

$$\eta = \frac{P_{useful}}{P_{delivered}} = 1 - \frac{Losses}{P_{delivered}} = 1 - \frac{AXL}{P_{delivered}} - \frac{ROTL}{P_{delivered}} - \frac{FRICL}{P_{delivered}} \tag{4}$$

Now, let's take a look at the individual losses.

Axial energy losses

The axial losses in a propeller are caused by the retardation of flow by the hull and acceleration of flow by the suction effect of the propulsor. The actuator disk model, where the propeller is represented by a disk in a non-viscous flow yields the following equation for axial losses in the far field:

$$AXL_i = \int\int \frac{1}{2}\rho\left[(u_{x0}^2 - U_0^2)\right]u_{x0}dA \tag{5}$$

These propeller axial losses are accounted for by the ideal efficiency η_i, which depends on the propeller thrust loading C_T :

$$\eta_i = \frac{TU_0}{AXL_i} = \frac{2}{1 + \sqrt{1 + C_T}} \tag{6}$$

where

$$C_T = \frac{T}{\frac{1}{2}\rho U_0^2 A_p} \tag{7}$$

and A_p is the propeller disc area

In open water conditions, for a real propeller, the non-uniform velocity distribution and viscous losses contribute to additional axial losses. These combined losses in a propeller-hull system are referred to as AXL_{WP} where WP refers to the wake of the self propelled condition. Axial losses cannot be easily separated in a real flow as the origin of the change in axial velocity cannot be traced [8].

Pressure losses

An additional term, expressed in terms of heat is present in the pressure loss term. The conversion of kinetic energy into heat caused by viscous dissipation results into an energy flux[8]. The pressure losses and the viscous dissipation term is referred to as Pressure losses in the following equation:

$$PRESSL_{WP} = \int\int_{A_{WP}} (p - p_0)u_{xWP}dA + \psi_{dissWP} \tag{8}$$

Rotational losses

These losses consists mostly of rotational losses for a propeller in open water conditions. The transverse velocities will plausibly be affected by the waterlines in the aft-body and the slope of the buttocks[8]. An out-flux of kinetic energy consists of radial and tangential velocity components.

$$ROTL_{WP} = \int\int_{A_{WP}} \frac{1}{2}\rho\left[u_{r0}^2 + u_{\phi 0}\right]u_{x0}dA \tag{9}$$

Like in axial losses, the non-uniformity in the wake also leads to an increase in transverse energy losses. This is caused by the finite number of blades and the radial load distribution over the blades of a propeller in open water[8].

$$P_D = AXL_{WP} + ROTL_{WP} + PRESL_{WP} \tag{10}$$

2.2 Energy Saving Devices

Energy saving devices(ESDs) are used to reduce the fuel consumption of a vessel at a given speed and draft. They do so by influencing one of more of the losses associated with the propeller. ESDs improve the propulsion efficiency by recovering losses from the propeller slip stream or by improving the inflow to the propeller. The possible gains to be obtained depend solely on the magnitude of losses present in the propulsion system which means that gains are case dependent. The influence of ESDs on the axial, frictional and rotational losses will be discussed in this subsection. ESDs can be installed either before, at or after the propeller as indicated by zones I, II and II respectively in figure 6.

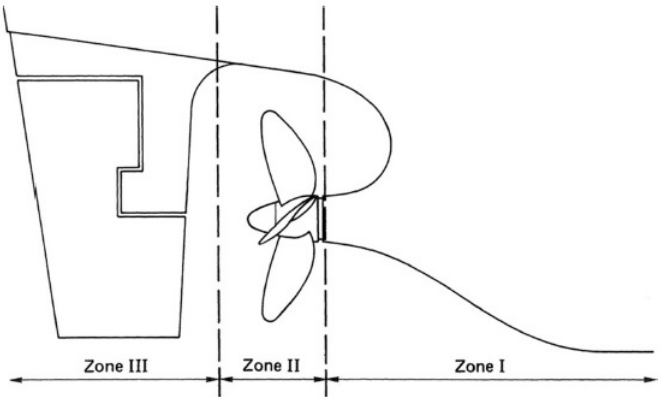

Figure 6: Different zones where an ESD can be placed[9]

Influence on Axial losses

They influence axial losses by making the inflow at propeller more uniform will lead to a more uniform outflow. This can help in reduction of axial losses. There are not many dedicated systems for reduction of axial losses. Pre-ducts for example can be considered as one of the devices which reduces axial losses[10].

Influence on Rotational losses

The rotational losses are influenced by stators mounted upstream or downstream of the propeller. This can be done by pre counter-rotating the flow or post capturing of the rotating flow. Also, propeller blades are more effectively and uniformly loaded, resulting in a reduction of rotation rate of the propeller at equal thrust[10].

Influence on Frictional losses

Not many effective systems are available for the reduction of frictional losses. In fact, most ESDs increase frictional losses by contributing to additional surface area[10].

2.2.1 Upstream ESDs

These devices are located in front of the propeller and aim to modify the flow that enters the propeller by manipulating the boundary layer or the flow itself.[10].

Pre-swirl stator

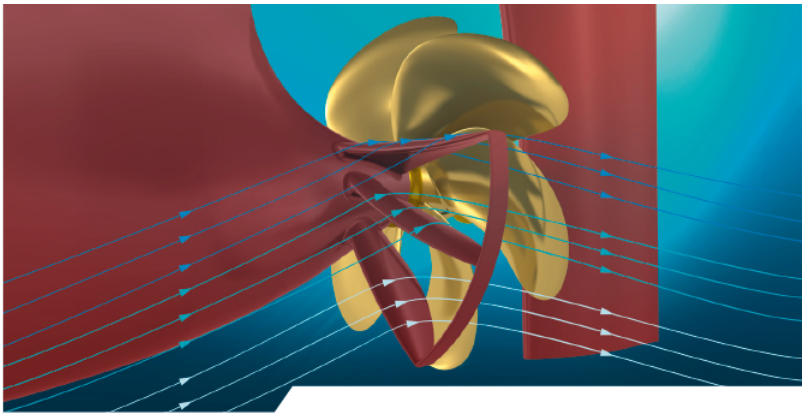

Figure 7: A pre-swirl stator by Wartsila

A pre-swirl stator generates a rotating flow in a direction opposite to that of which the propeller does. This leads to the flow leaving the propeller disc at a minimum momentum in circumferential direction. Thus, less kinetic energy is spent to produce a certain thrust. Terwisga et al.[2] describe the working principle of a preswirl stator as the improvement in performance of propeller by realigning the total force vector through pre-swirl.

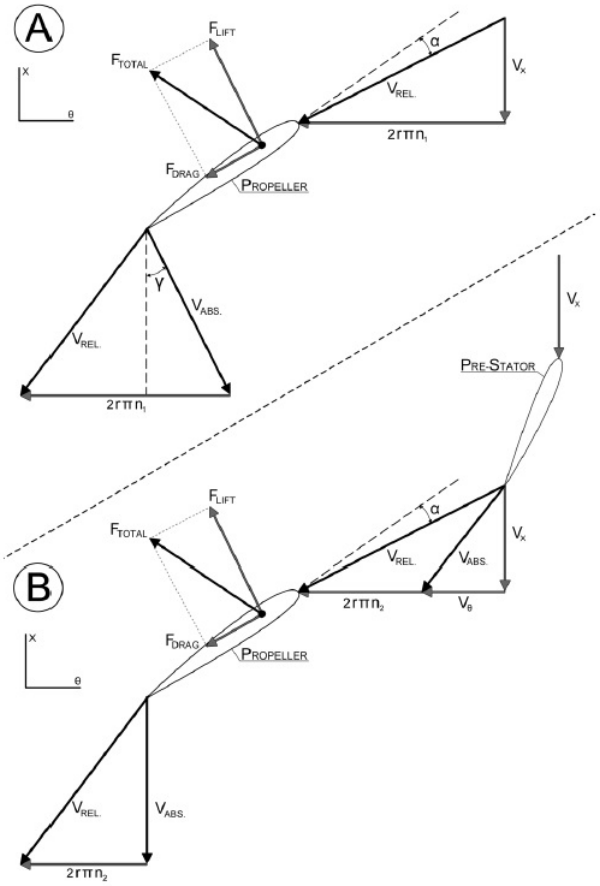

Figure 8: Velocity and Forces of a **A.** propeller section and **B.** a propeller section with preswirl stator[2]

Figure 8 shows velocity and forces of a propeller section with and without a pre-swirl device. The figure consists of two parts. Diagram A is without the pre-swirl device whereas diagram B is with the pre-swirl device. The propeller blade section experiences a certain angle of attack resulting in a total force vector acting on it as shown in the figure. The total force vector can be broken up into forces in axial and tangential directions. The force in axial direction represents the thrust T and the force in tangential direction times the local radius of the blade section represents the torque Q. The velocity in the earth fixed reference frame V_{ABS} has a tangential component(A) behind the propeller, which gives an acceleration to the fluid and does not contribute to the propulsion of the ship. It creates rotational kinetic energy losses. A pre-swirl stator counters this by introducing a pre-swirl(B) without changing the angle of attack and consequently the total force vector also remains unchanged. This allows the propeller to generate the same thrust at a lower rpm and hence reduces the power demand. It can also be said that a pre-swirl stator allows the propulsion system to generate more thrust at the same rpm than it would without the stator. Terwisga et al.[2] assessed the performance of a pre-swirl stator, called the Blade efficiency improving Stator Duct (BSD). They did this by conducting RANS simulations and found reduction of power by 4.1% at model scale and 3.4% at full scale.

Pre-duct

A Pre-duct as the name suggests, is a duct in front of the propeller and can be seen in figure 9. The working mechanisms for pre-duct as hypothesized by Terwisga[8] are as follows:

1. Increasing the mass flow through the propeller, resulting in lower axial losses by propeller.

2. Use of propeller hull interaction to reduce axial losses through increase of wake fraction or decrease of

Figure 9: Preduct [10]

thrust deduction factor.

3. To reduce effects of non-uniformity.

Studies conducted on pre-ducts by Kim et al., Shin et al. on different kinds of pre-ducts result in power reduction from 3% to 6%[11][12].

Mewis Duct

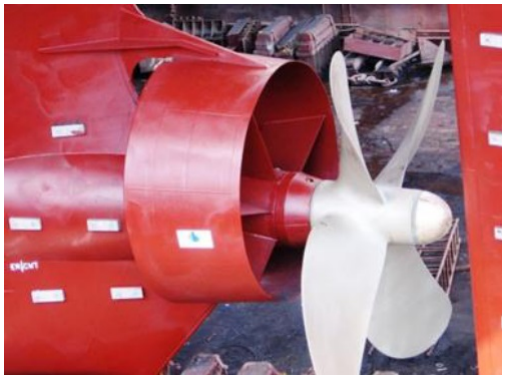

Figure 10: Mewis Duct [13]

A Mewis duct (figure 10) can be thought of as a combination of a pre-duct and a pre-swirl stator. The device reduces the rotational losses in the propeller slipstream and increases the mass flow through propeller by influencing the flow going into the propeller.

Figure 11 shows the results of self-propulsion test of 64 projects (as on September 2012) with and without MD fitted in 9 different towing tanks, plotted over the thrust loading coefficient C_T revealed that the average power reduction is 6.3%, in design draft 5.7% and in ballast draft 7.3%[13]. The Mewis Duct is suited to ships whose propeller thrust coefficient C_T is typically greater than 1 and speed less than 20 knots. This encompasses small container vessel, vessels with high block coefficients, multi-purpose carriers, all tankers and bulk carriers. Optimisation of the ESD is case dependent[14].The installation position, radius, angle of attack of the inner fins, profile of the inner fins and outer duct also have a huge influence on its performance. These parameters should be optimized to achieve better energy saving effects[15].

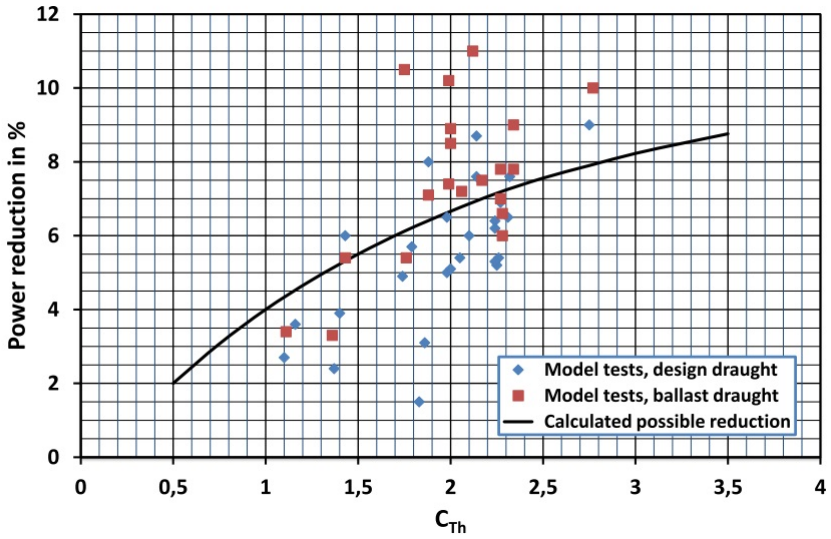

Figure 11: Power reduction by Mewis Duct [13]

Wake Equalising Duct

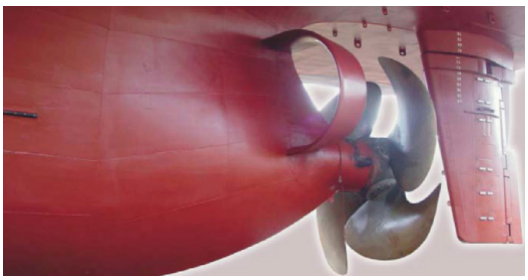

Figure 12: Wake equalising duct [16]

One of the ESDs used widely in ships is the wake equalising duct (WED). The working of WED is similar to a pre-duct. It consists of two aerofoil sectioned half-ring ducts integrated to the hull in front of upper region of the propeller. Some important parameters of the WED are the angles of duct axis to ship's centre line plane, longitudinal positions, inner diameters, profile section shapes, angles of section to duct axis and lengths of the half-ring ducts[16]. It is assumed that the WED accelerates the inflow of the upper region of the propeller where the flow is slow relative to the lower region of the propeller, and improves the uniformity of the wake over the propeller disc, so that the propeller efficiency is increased. A well designed WED reduces the the amount of flow separation at the aft and generates an additional thrust[16]. The uniform wake reduces the vibrational forces on the propeller and the improvement in the flow to the rudder is also beneficial for steering. Efficiency gains upto 9% have been reported for a WED[16].

2.2.2 ESDs at propeller

These devices operate directly at the propeller.

Grim vane wheel

A Grim vane wheel is a second propeller located immediately behind the propeller and it is driven by the

Figure 13: A grim Vane Wheel [17]

wake of the main propeller. An increase in propeller diameter is beneficiary for efficiency. A concept to obtain an increased diameter without increasing the diameter of the main propeller is the Vane wheel. The inner part of the vane wheel (impeller) has a pitch such that the vane wheel is driven by the wake of the main propeller. The outer part of the blades of the vane wheel, the propeller part, has a different pitch, which causes the vane wheel to generate thrust of the main propeller. The concept was designed by Grimse Leitrad and is patented. A vane wheel reduces the axial and tangential velocity in the wake of the main propeller. However, they are subjected to strong fluctuations in loading. Problems with the strength of the blades have been encountered frequently and this led to its limited application [18].They are expensive and can be affected by cavitating tip-vortex. Also, no new installations are known after the accident of Queen Elizabeth 2[10].The main function of the vane is to extract energy from the propeller slipstream in the turbine portion and to convert this energy into additional thrust in the propeller portion[17]. The diameter of the vane wheel is about 20% larger than that of the propeller and the distance between propeller and vane wheel is about 25% of the propeller diameter. Usually, the vane wheel has more than six blades and rotates at 30%-50% of the propeller rpm. The vane wheel can lead to power savings of 5% making it quite efficient. However, as mentioned earlier, it is not used anymore due to fears that the thin blades might get damaged and wave loads can also cause damage to the hub and blades[17].

Nozzle or Ducted propeller

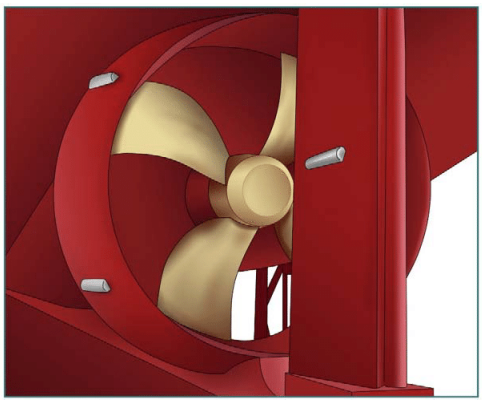

Figure 14: A Nozzle

A ducted propeller is a propeller fitted with a non-rotating nozzle. Nozzle or ducted propellers are usually

used when high efficiency is required at low speed of the vessel, for example, tug boats or certain types of off-shore vessels[19]. It is used to improve the efficiency of the propeller and is especially used for heavy loaded propellers or propellers with limited diameter. Another positive effect of the nozzle is to suppress the formation of blade tip vortices thus also reducing some further losses. The nozzle can generate about 50% of the thrust in bollard conditions [10]. They can be significantly more efficient than unducted propellers at low speeds. Tugs and fishing trawlers are common examples.At high speeds, viscous losses become dominant i.e the resistance is larger than positive thrust. Therefore, for high speed application or lightly loaded propellers(low C_T), a nozzle is not recommended.

Propeller Boss Cap With Fins

Figure 15: Propeller Boss Cap with fins[20]

Propeller Boss Cap Fin (PBCF) is one of the most popular ESDs because it is relatively easy to manufacture and install which makes it cost effective[20]. More than 2000 sets have been sold since its first introduction in 1987[21].Conventional propellers experience hub vortex loss which is a stream of strong vortex flow that is usually generated near the propeller hub. The induced drag generated by hub vortex leads to decrease of efficiency of a propeller near the hub. PBCF helps in weakening of these hub losses by diverting the flow behind bow caps[22]. This also eliminates the low pressure region caused by the hub vortex, thereby reducing the drag. This elimination of the low pressure region can be seen clearly in figure 16.

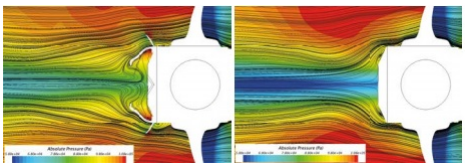

Figure 16: Pressure distribution with (left) and without PBCF [23]

Full scale trials conducted on an Aframax tanker by Hansen et al. correlated with the model scale test results and predicted power savings were 3.5%, which meant a payback time of about 6 months[24].

2.2.3 Downstream ESDs

These are typically located behind the propeller and they take advantage of the kinetic energy found within the swirl of the slipstream and generate additional thrust from that kinetic energy [10].

Post-swirl stator

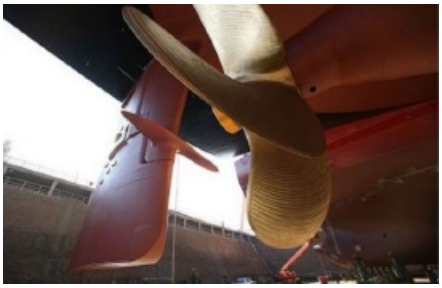

Figure 17: Post-swirl Stator [10]

These are fins located aft of the propeller and are usually placed on the rudder or rudder support. They are located on the shaft height and can be of single or multi-fin configuration. This concept aims at recovering kinetic energy rotating flow behind the propeller. The fins need to be designed in combination with the rudder[10].

Rudder bulb hub cap

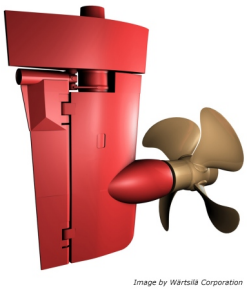

Figure 18: Rudder Bulb Hub Cap

The rudder bulb hub cap is a combination of a propeller, streamlined fairing cap and a rudder system with a rudder bulb. The fairing cap and rudder are designed to reduce the propeller hub losses[10]. It also improves the hull efficiency by making the wake distribution more uniform. Flow separation and hub vortex are some of the issues when dealing with the slipstream of propeller. These lead to kinetic energy loss and vortex cavitation. The rudder bulb is intended to improve propulsive efficiency by weakening the hub vortex and preventing the flow separation. The rudder bulb system consists of the hub cab and the bulb attached to the rudder[25]. Okada et al. found a gain of 3.5% - 4.1% in propulsive efficiency in their study[26].

3 Outcome of Literature Review

Table 3 shows the average possible gain in propulsive efficiency with the help of the ESDs.

S.No	ESD	Articles	Gain	Part-load
1	Pre-Swirl Stator	8	3%-5%[10][27]	?
2	Pre-Duct	5	0%-7%[10][27]	?
3	Mewis Duct	7	3%-8%[14][27]	?
4	Grim Vane Wheel	3	5%-10%[10]	?
5	Nozzle	3	5%-10%%[27]	?
6	Propeller Boss Cap With Fins	8	0%-4%[23]	?
7	Post-Swirl Stator	3	2%-6%[10][27]	?
8	Rudder Bulb Hub Cap	5	0%-6%[10][27]	?

Table 3: Possible gain in propulsive efficiency with ESD

It can be seen in the table that there is literally no information available on the performance of ESDs.

S.No	ESD	Cavitation	Cost	High Seas
1	Pre-Swirl Stator	?	250-300k[28]	?
2	Pre-Duct	?	?	?
3	Mewis Duct	-[29]	275k[28]	+[29]
4	Grim Vane Wheel	?	525k-575k[28]	?
5	Nozzle	?	?	?
6	Propeller Boss Cap With Fins	-[30]	100k-150k[28]	?
7	Post-Swirl Stator	?	100k-150k[28]	?
8	Rudder Bulb Hub Cap	-[26]	250k-300[28]	?

Table 4: Comparison of ESDs based on cavitation, cost and high seas performance

The estimated cost of the ESDs are taken from [28]. The - sign in the cavitation column indicates that PBCF and rudder bulb hub cap reduce the hub vortex cavitation according to Mizzi et al.[30] and Okada et al.[26] respectively. According to Mewis[29], a Mewis duct reduces cavitation and also improves performance in high seas, indicated by the - and + sign respectively.

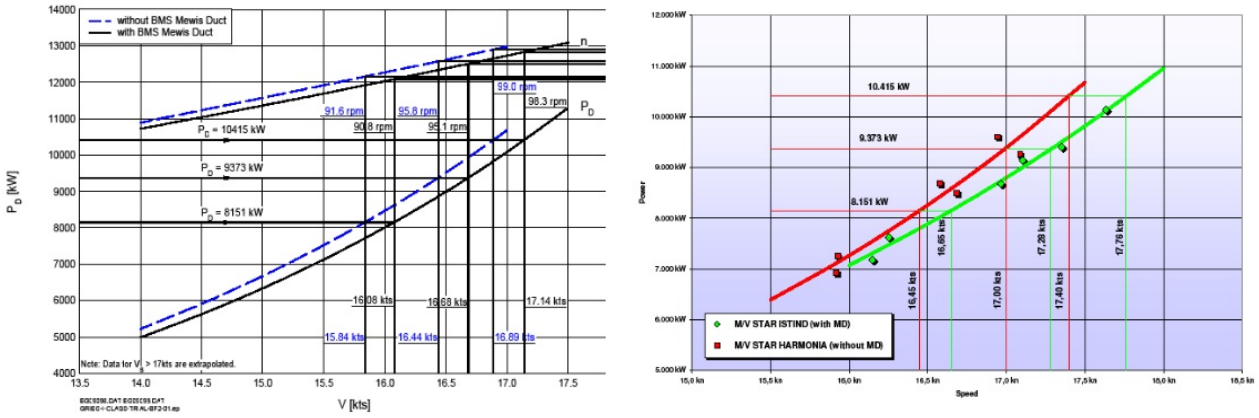

(a) Model test

(b) Full scale trial

Figure 19: Test results of STAR ISTIND[29]

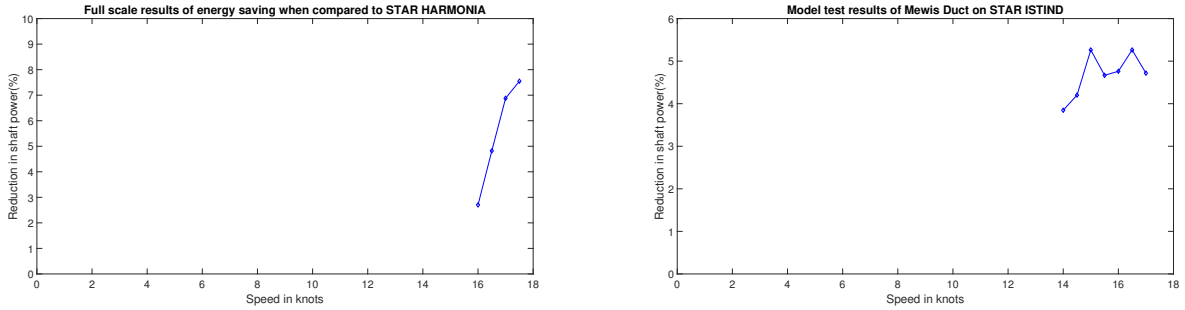

(a) Full-scale comparison

(b) Model Test

Figure 20: Energy saving of STAR ISTIND[29]

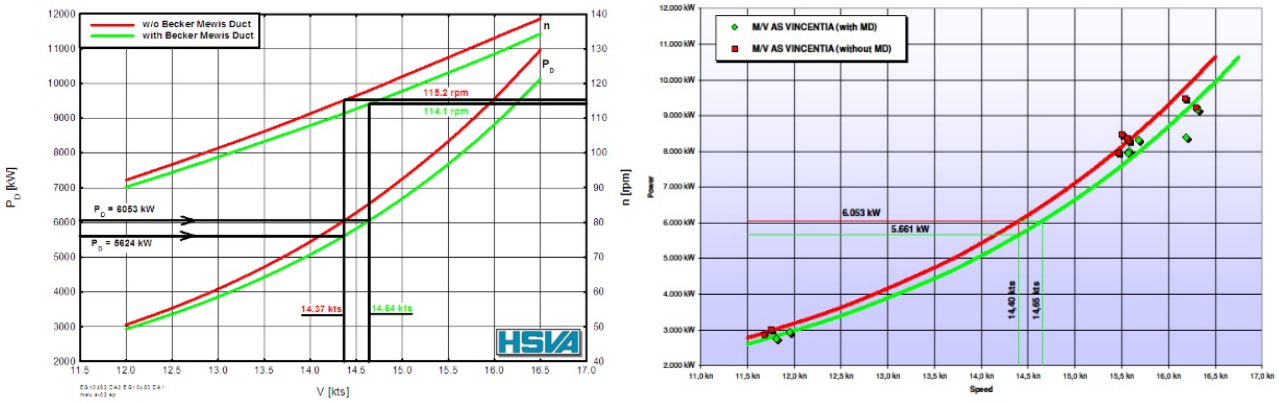

(a) Model test (b) Full scale trial

Figure 21: Test results of AS VINCENTIA[29]

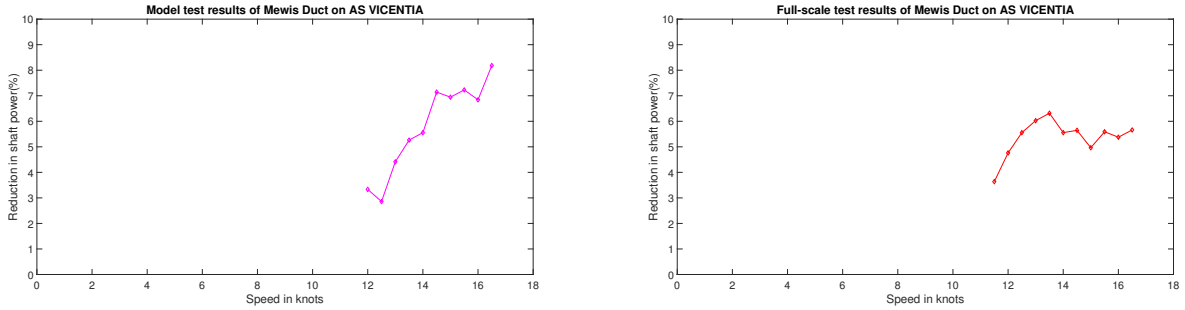

(a) Model test (b) Full-scale trials

Figure 22: Energy saving of AS VINCENTIA[29]

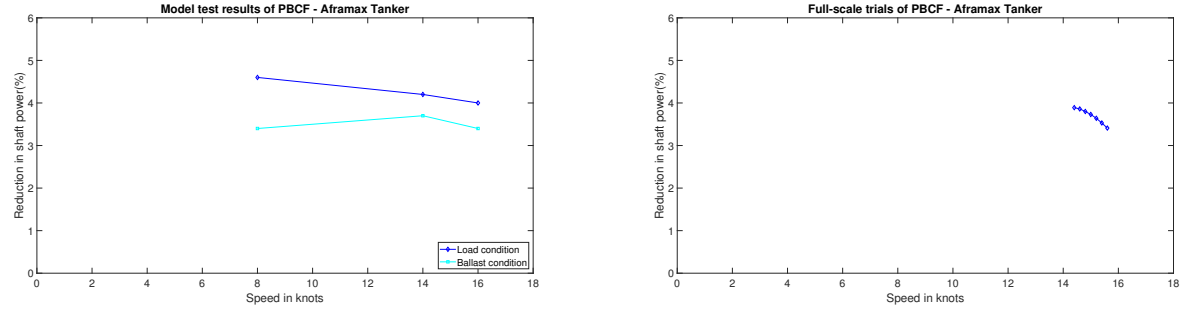

(a) Model test (b) Full-scale trials

Figure 23: Energy saving of an AFRAMAX Tanker[29]

To give an idea about the missing information on the performance of upstream ESDs in part-load conditions, some examples are shown. STAR ISTIND of Grieg star shipping, a general cargo vessel with a deadweight of 45000 was the first vessel to install mewis duct in full scale in September 2009 and results of the model tests are shown in figure 19a. The full scale speed-power analysis of sister ships M/V STAR ISTIND and M/V STAR HARMONIA are shown is figure 19b. Model test and full-scale trial results of AS VICENTIA, a supramax bulk carrier with a deadweight of 57000 are shown in figure 21. The energy saving effect of the above mentioned vessels are also shown in figures 20, 22 and 23. It can be seen that the comparison with and without the ESD is done only for speeds close to design point. This does not provide any information on how these ESDs will act in part-load conditions. The performance of Pre-duct, Mewis Duct and Preswirl Stator in part-load conditions will be discussed in the next section - 3.1.

3.1 Part load performance

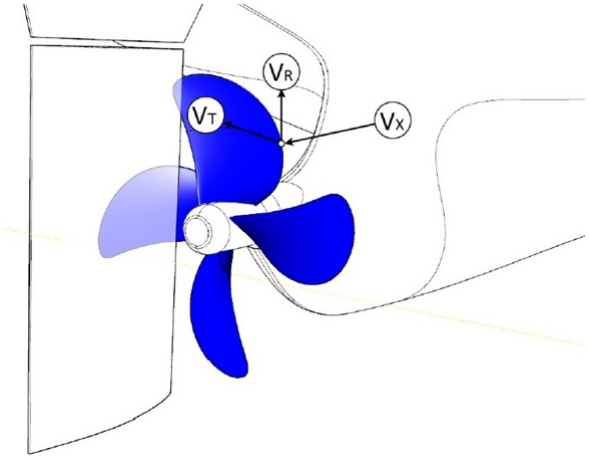

Figure 24: Induced Velocities[27]

Most of the ESDs are tested at the ship's design speed and design draft. A few of them like Mewis Duct and Pre-swirl stator were tested at loaded condition and ballast condition but it is not very clear whether these ESDs will be beneficial for a range of speeds or in part-load conditions. Also, test results from different authors give different results, the standard deviation being approximately 2% in most cases. This is to be expected as they are always uncertainties involved with model tests, CFD results and full scale trials. In theory, there exists no formula to predict the performance of ESDs for a range of speeds. The energy saving may increase or decrease with speed. This has already been seen in the various model tests and full-scale trials of different kinds of ships. Up until now, it is clear that the effect of energy saving comes through influencing the energy losses in the flow. This is true as the momentum flux between in and out-flow plane remains unchanged as long as the ship is moving at a steady speed. And ESDs cannot produce a net change in this momentum flux.

The losses associated with the propeller are axial, rotational and frictional. An investigation carried out by Molland et al.[5] on a propeller with 4 blades with pitch ratio of 1, BAR = 0.7 for a range of J values yielded the propeller loss diagram shown in figure 25. Here, it can be clearly seen that the axial losses decrease significantly with the increase in the advance coefficient J. The frictional losses increase with J whereas as the rotational losses, like axial losses, decrease.

The postulation will focus on three ESDs: Pre-duct, Preswirl stator and Mewis duct. Let's take pre-swirl as an example here. The working principle of a pre-swirl stator is to improve the performance of the propeller by realigning the total force vector[2]. This is described in detail in section 2.2.1 with the help of figure 8. A pre-swirl stator can help the propulsor generate the same thrust at a lower rotation rate than it would without

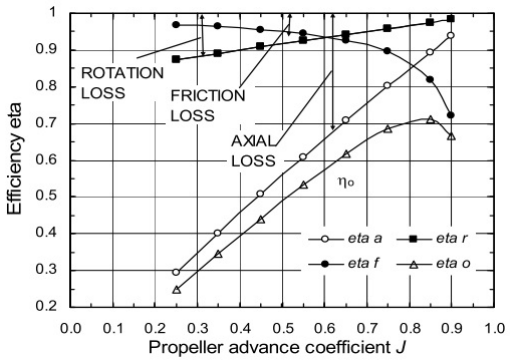

Figure 25: Losses associated with a propeller[5]

the pre-swirl device. In other words, it can generate more thrust at the same rotation rate. With this being said, if the classical approach is used to analyse the performance of the propeller with a pre-swirl stator, an increase in thrust also increases the thrust coefficient K_T. An increase in K_T leads to a decrease in open water efficiency when an open water diagram is referred. Table 5 shows the results of the classical approach from GRIP (Green Retrofitting through Improved Propulsion) project which was funded by the European Union. Figure 26 shows the relative difference in percentage in the efficiencies of the classical approach.

		Rel. Difference
Openwater Eff.	η_o	0.947
Rel. Rotative Eff.	η_R	0.985
Hull Eff.	η_H	1.119
Total Improvement	η_D	**1.044**

Table 5: Results of the classical approach from GRIP project[27]

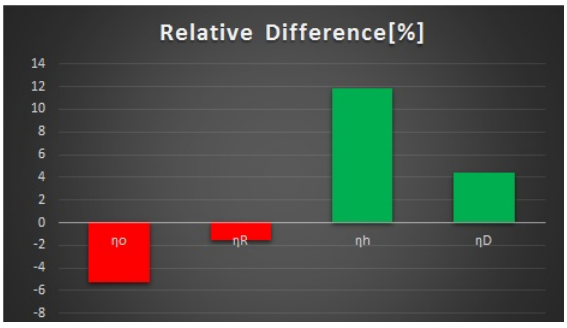

Figure 26: Results of the classical approach from GRIP project[27]

The classical approach to analyse propeller performance is :

$$\eta_D = \frac{P_E}{P_D} = \frac{(R-F)V_s}{2\pi n Q_B} = \frac{T_o V_s (1-w)}{2\pi n Q_o} \frac{Q_o T_B}{T_o Q_B} \frac{(1-t)}{(1-w)} = \eta_o \eta_r \eta_h \tag{11}$$

where η_D is the propulsive efficiency and is defined as the ratio of the effective power to the power absorbed by the propeller. η_o, η_r, and η_h are the open water efficiency, relative rotative efficiency and hull efficiency. Here o depicts the open water condition and B represents the 'behind condition'. The relative rotative efficiency

also decreases which could be due to decrease in K_{Qo} or an increase in K_{QB}. Figure 27 depicts the the open water and self propelled condition (in-behind condition). Subscripts SP in figure 27 and B in equation 11 mean the same. The hull efficiency increases notably, suggesting that a pre-swirl stator improves the propeller-hull interaction. This leads to the conclusion that the wake fraction increases considerably but the pre-swirl stator hardly affects the mean axial velocity[2]. This approach does not lead to an understanding of the working principle of a pre-swirl device.

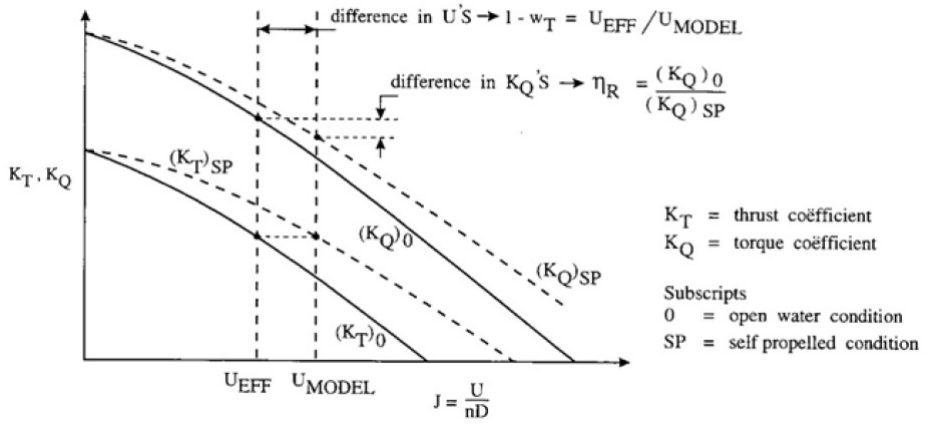

Figure 27: Efficiency Analysis[27]

Terwisga et al.[2] propose an alternative way to analyse the performance of ESDs at constant speed. They use 'behind ship' propeller performance without ESD rather than using 'open water' component, the hull component and the interaction term. They define the efficiency of the propulsor (propeller and preswirl device) as:

$$\eta_{ESD} = \frac{n_0 Q_{B0}}{n_1 Q_{B1}} \frac{T_{B0}}{T_{B0}} \frac{T_{B1}}{T_{B1}} = \frac{T_{B1} n_0 Q_{B0}}{T_{B0} n_1 Q_{B1}} \frac{T_{B0}}{T_{B1}} = \Delta\eta_{prop.eff} . \Delta\eta_{interaction} \tag{12}$$

where

$$\Delta\eta_{prop.eff} = \frac{n_0}{n_1} \frac{T_{B1} QB0}{T_{B0} QB1} = \Delta\eta_{Bladeloading} \Delta\eta_{Bladeefficiency} \tag{13}$$

Here, subscript 0 refers to the configuration without ESD and 1 represent the configuration with ESD. The first term represents the efficiency change in the propeller action, while the second is a measure of the improvement of the interaction between propeller and hull. The propeller efficiency can be broken down into blade loading and blade efficiency. The change in blade loading efficiency, which is the ratio in rotation rates, is a measure of the total increase in thrust at identical rpm. The blade efficiency expresses the change in the orientation of the total lift vector and radial load distribution [2]. The blade effectiveness or the blade efficiency is defined as the dimensionless ratio of thrust and torque coefficient, and changes with the angle of attack.

$$\eta_{Bladeefficiency} = \frac{K_T}{K_Q} = \frac{T.D}{Q} \tag{14}$$

Table 6 shows the results of the alternative approach from GRIP project, where η_{WP} denotes the blade loading efficiency, $\eta_{T/Q}$ denotes the blade efficiency and η_{INT} denotes the interaction efficiency which is basically the thrust deduction factor. Figure 28 shows the relative difference in percentage in the efficiencies of the alternative approach.

		Rel. Difference
Blade loading	η_{WP}	1.043
Blade efficiency	$\eta_{T/Q}$	1.016
Interaction	η_{INT}	0.985
Total Improvement	η_D	**1.044**

Table 6: Results of the alternative approach from GRIP project[27]

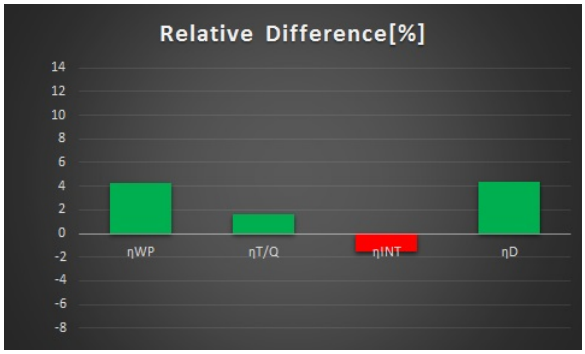

Figure 28: Results of the alternative approach from GRIP project[27]

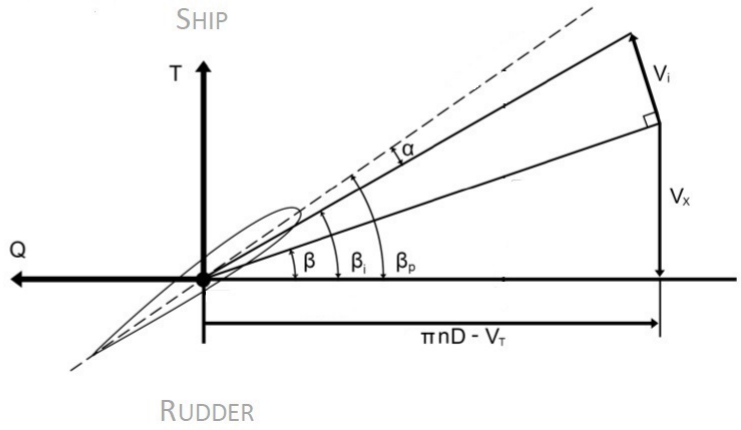

Figure 29: Velocity and Forces of a propeller blade section at constant radius[2]

Figure 29 shows the velocity and forces of a propeller blade section. Here α is the angle of attack, β_P is the pitch angle, which is the angle between the pitch line and the plane perpendicular to the shaft. Angle of attack α will be higher for a higher pitch angle β_P. If the induced velocities are neglected, the angle of attack can then be defined as the difference in hydrodynamic pitch angle β and the propeller pitch angle β_P. Thus, a change in α is equal to change in β,

$$\alpha \sim arctan\left(\frac{V_x}{2\pi nr - V_T}\right) \tag{15}$$

Terwisga et al.[2] made some conclusions from the equation 15.

1. A change V_T will have the most influence on angle of attack α at the inner radii as the local rotational velocity is relatively small in that region. The advance velocity has the most impact on angle of attack α at the outer radii.

2. The angle of attack and consequently the local efficiency decreases for a positive V_T

To sum up, increasing the angle of attack leads to an increase in the blade efficiency. A pre-swirl stator can maintain the same angle of attack at a lower rotation rate, resulting in an increase in efficiency. This is explained in section 2.2.1. Increasing angle of attack α tilts the total force vector in a more suitable direction, increasing the thrust component and reducing the torque component or leads to reduction in the thrust to torque ratio. This can be seen in figures 30, 31, 32. The blade efficiency can particularly be increased at the inner radii because the largest variation of angle of attack α occurs there. From equation 15, it can seen that the angle of attack will increase with increase in the ratio of advance velocity to the product of rotation rate and diameter of the propeller. According to Stapersma et al. [31], the physical importance of J is that it is proportional to the tangent angle between advance velocity and circumferential speed, it is therefore, proportional to the hydrodynamic pitch angle β. And, it has already been established that a change in angle of attack is equal to change in the hydrodynamic pitch angle (ref. equation 15). Thus, it is postulated that the energy saving effect of a pre-swirl stator increases linearly with increase in advance coefficient J.

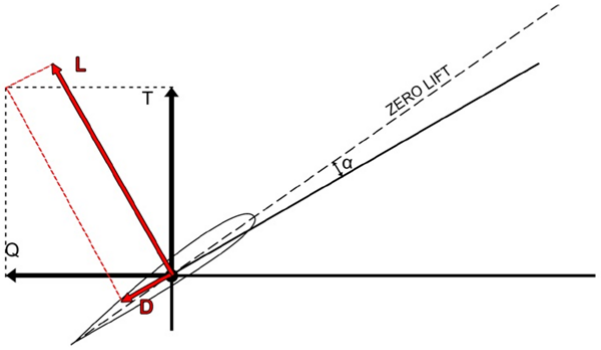

Figure 30: Propeller inflow[27]

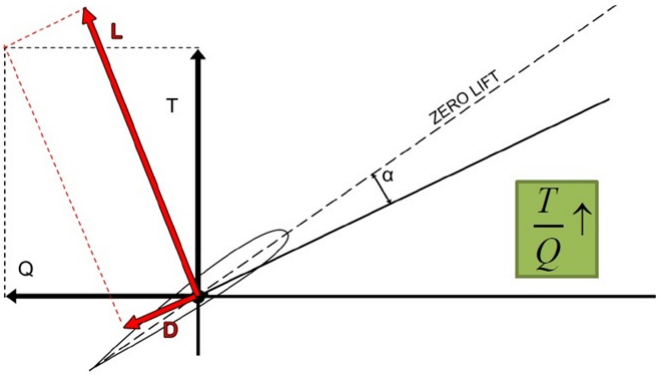

Figure 31: Propeller inflow - An increase in angle of attack[27]

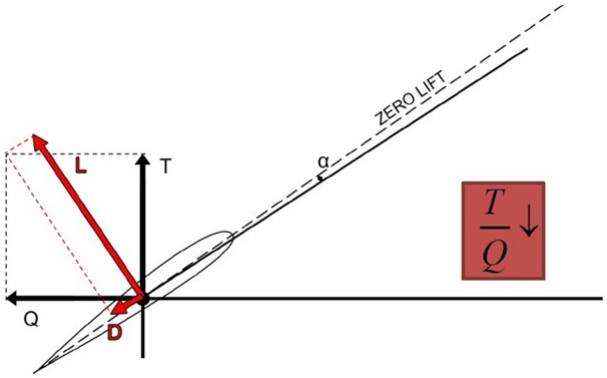

Figure 32: Propeller inflow - A decrease in angle of attack[27]

A pre-duct works on the same principle as a nozzle i.e it increases the mass flow through the propeller resulting in reduction of axial losses [8]. Also, a pre-duct like a nozzle, will plausibly have better performance at higher thrust loading coefficients (low J). Therefore, it is postulated that both pre-duct and mewis duct are expected to have higher axial kinetic energy loss savings at lower advance coefficients (J). However, a mewis duct will not have as high energy savings at lower J values as a pre-duct, as it is combination of a pre-duct and pre-swirl stator. The stator fins of a mewis duct are expected to have a similar effect on rotational losses as a pre-swirl stator does. A linear approach is adopted for these two ESDs as well. Also, the frictional losses increase because of these upstream ESDs as they are an added appendage. In section 4, a mathematical model is presented to predict the performance of these upstream ESDs for a range of speeds. However, it is important to understand that this is based on a postulation and model tests and CFD self-propulsion simulations must always be carried out before implementing these devices on a ship.

3.2 Why are ESDs used only for ships with high block coefficient?

The higher wake fraction at the aft due to the high blockage effect of a full form hull shape has a greater potential for exploiting energy saving devices, when compared to a slender hull form such as a container vessel[32].

3.3 What is the effect on carbon emissions and EEDI?

Take for example, an engine of 30,000 kW and state-of-art fuel consumption rates, annual fuel costs for one vessel can be expected to be about 4.8M€ based on prices in 2011. A 5% power reduction will lead to savings of about 240k€ per year, or, in ecological terms, a reduction of CO_2 emissions of about 5200 ts per year. If a fleet of 100 vessels is considered, then this would yield in the reduction of almost half a million ton of CO_2 emission[33]. ESDs when designed properly, definitely lead to a reduction of CO_2 emissions and improve the EEDI score of the vessel. In existing ships, it can help in meeting the EEDI requirements in the immediate future(2020) and in newly built ships, it can help in meeting the EEDI requirements of 2030 with a combination of the right engine and an optimized propeller.

3.4 Which is the State-of-art ESD?

ESDs are tailor-made for a specific ship and most of them reduce the same amount of power when designed optimally. CFD and model tests, cost and performance history play a huge role in deciding which ESD is best suited for a particular ship. The most popular ESDs are Mewis Duct, Propeller boss cap fins and wake equalising duct. Pre-swirl stators are also quite popular.

A combination of multiple devices is not recommended as they may not necessarily lead to additional savings. In fact, some devices may actually remove the flow regimes upon which other devices work on[10]. A thorough investigation should be done before using a combination of ESDs for a vessel.

3.5 What is the scope of hull form(s) to be analysed?

Most ESDs mentioned in this thesis are effective for ships with high block coefficient. Their effectiveness varies from ship to ship and it is of utmost importance to choose the right ESD, otherwise, they can have a negative effect on the propulsive efficiency. The ESDs upstream of the propeller are best suited for vessels with high block coefficient and speeds less than 20 knots. This encompasses Bulk carriers, tankers, small container vessel and multi-purpose carriers. Nozzles are used mostly in tugs and fishing trawlers. Propeller boss cap fins and ESDs downstream of the propeller can be used on ships with high block coefficient as well.

4 Simplistic model for propeller partial efficiencies

A mathematical model of the propeller (figure 25) discussed at the beginning of section 1.4 is presented where the effect of a pre-duct, preswirl stator and a mewis duct is analysed. Table 7 shows the efficiencies with respect to advance coefficient J. Here η_a is the axial efficiency, η_r the rotational efficiency, which accounts for losses due to fluid rotation induced by propeller, and η_f, the frictional efficiency accounts for losses due to blade friction drag. η_o is the open water efficiency.

$$\eta_0 = \eta_a . \eta_r . \eta_f \tag{16}$$

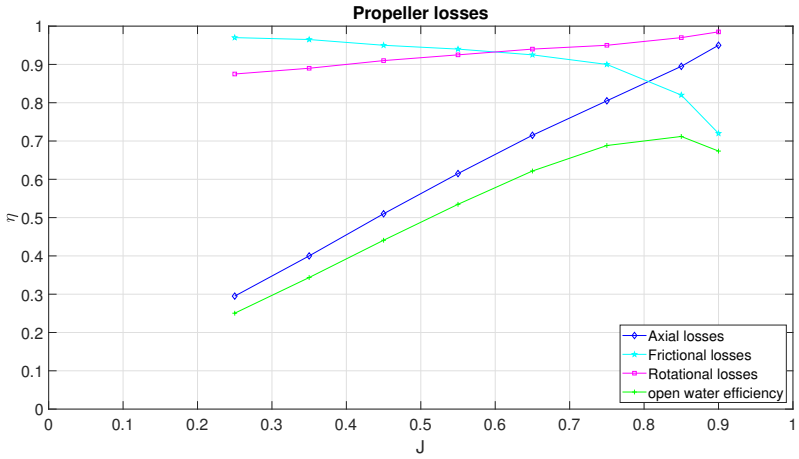

Figure 33: Propeller losses [5]

J	η_a	η_r	η_f	η_o
0.25	0.295	0.875	0.97	0.2504
0.35	0.4	0.89	0.965	0.343
0.45	0.51	0.91	0.95	0.441
0.55	0.615	0.925	0.94	0.534
0.65	0.715	0.94	0.925	0.622
0.75	0.805	0.95	0.9	0.688
0.85	0.895	0.97	0.82	0.712
0.9	0.95	0.985	0.72	0.674

Table 7: Propeller losses [5]

Assumptions for the model

1. Energy saving devices are designed optimally.
2. Frictional losses increase linearly with increase in J(advance coefficient) and are assumed to be 2% at max J for a pre-duct and pre-swirl stator and 3% at max J for a mewis duct.

3. The average gain of a pre-swirl device is assumed to be 4% (see table 3). A pre-swirl has higher rotational gain than the average gain shown in table 3. This is a valid assumption as a pre-swirl device increases frictional losses due to its additional surface area. Therefore, in order to obtain an average gain of 4% (table 3) or close to it, a rotational gain η_r of 8.6% is assumed.

4. Similarly, a pre-duct has higher axial gain than the average gain (3.5%) shown in table 3. Again, this is a valid assumption as a pre-duct increases frictional losses due to its additional surface area. Therefore, an axial gain η_a of 5.4% at max J is assumed and the axial gain is decreases with increasing J.

5. A Mewis duct has higher rotational gain than axial gain. The stator fins are expected to increase the rotational gain but also act as an obstruction when it comes to increasing the axial gain. So, the axial gain for a mewis duct is expected to be less than that of a pre-duct.

In this model, the overall gain in efficiency is shown in propeller loss diagrams to have a better idea about the improvement of efficiency by the ESDs. Also, the gains found out by the literature review (table 3) are gains in the propulsive efficiency.

Pre-swirl Stator

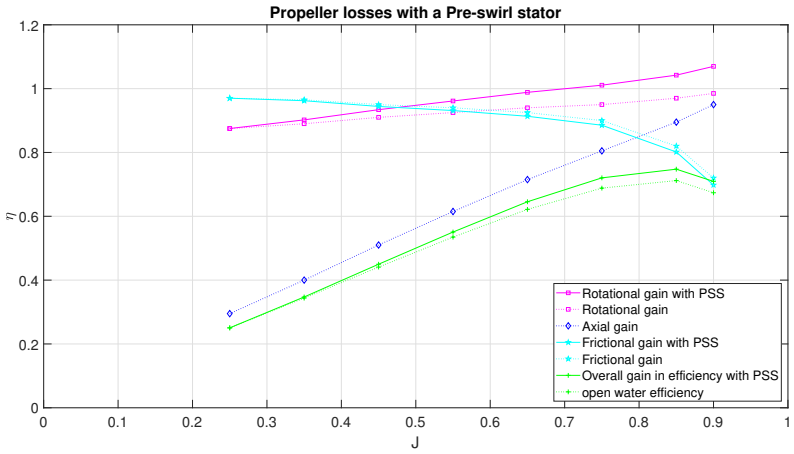

Figure 34: Influence of Pre-swirl stator

A pre-swirl stator influences the rotational losses of a propeller. In figure 34, the purple dotted line indicates the rotational losses of a propeller without any energy saving device, whereas the purple line shows the effect a pre-swirl stator has on rotational losses. The efficiency gain has been calculated by taking the percentage decrease in the losses at each advance coefficient(J) value from figure 25 and multiplying by a factor increasing linearly with advance coefficient. The same is done for increase in frictional losses with increasing J as the ESD is an added appendage and leads to increase in frictional losses.

Table 8 shows the decrease in rotational losses due to a pre-swirl stator. The first column in the table represents the difference in rotational efficiencies η_r between two consecutive J values from table 7. The second column is the percentage of this difference. The energy saving factor f_{esd} is dimensionless and comes from table 10 where rotational gain and frictional loss is applied at the J values as shown in the table and expressed in percentage. Average savings of a pre-swirl stator is taken as 4% and is taken from table 3. A pre-swirl device hardly affects the axial velocity which means that it will only have a minor affect on axial losses. It is assumed that this minor effect is negligible. It is also assumed that to get an average overall efficiency gain of 4%, a gain higher than 4% will be obtained for η_r, since frictional losses will increase with increasing J due to the presence

of the pre-swirl i.e η_f will decrease as J increases. Thus, for this propeller, it is assumed that there will be a gain of 8.6% in η_r and a loss of 2% in η_f at max J when a pre-swirl device is installed. The second column in table 10 shows the linear increase of rotational gain as J increases and these values are then multiplied with the corresponding values of the second column from table 8 to obtain f_{esd}. The values from f_{esd} are then added to η_r from table 7 to give η_{rpss}, which represents the rotational efficiency of the propulsor (propeller and pre-swirl stator). η_{fpss} in table 9 is calculated in a similar manner, the only difference being that the frictional losses increase with increasing J which is indicated in table 10 by the 'Fric loss' column. Table 11 shows the efficiency of the propulsor (propeller and pre-swirl stator) which is denoted by η_{pss}. η_{pss} is calculated by using the formula : $\eta_{pss} = \eta_a.\eta_{rpss}.\eta_{fpss}$

RotL	$\frac{1-RotL}{100}$ (%)	f_{esd}	$\eta_{r_{pss}}$
0.015	0.00985	0.012101	0.902101
0.02	0.0098	0.02408	0.93408
0.015	0.00985	0.036304	0.961304
0.015	0.00985	0.048406	0.988406
0.01	0.0099	0.060814	1.010814
0.02	0.0098	0.07224	1.04224
0.015	0.00985	0.08471	1.06971

Table 8: Decrease in rotational losses due to pre-swirl

FricL	$\frac{1-FricL}{100}$ (%)	f_{esd}	$\eta_{f_{pss}}$
-0.005	0.01005	-0.00287	0.962129
-0.015	0.01015	-0.0058	0.9442
-0.01	0.0101	-0.00866	0.931343
-0.015	0.01015	-0.0116	0.9134
-0.025	0.01025	-0.01464	0.885357
-0.08	0.0108	-0.01851	0.801486
-0.1	0.011	-0.022	0.698

Table 9: Increase in frictional losses due to pre-swirl

J	Rot. gain(%)	Fric loss(%)
0.35	1.228571	-0.28571
0.45	2.457143	-0.57143
0.55	3.685714	-0.85714
0.65	4.914286	-1.14286
0.75	6.142857	-1.42857
0.85	7.371429	-1.71429
0.9	8.6	-2

Table 10: Gains applied on a Pre-swirl stator

η_o	η_{pss}	η_{o_+}	η_{o_-}
0.250381	0.250381	0.260497	0.240466
0.34354	0.347175	0.361201	0.333427
0.440895	0.449799	0.467971	0.431987
0.534743	0.550612	0.572857	0.528808
0.621693	0.645509	0.671588	0.619947
0.688275	0.72042	0.749525	0.691891
0.711883	0.74763	0.777834	0.718024
0.67374	0.709325	0.737981	0.681235

Table 11: Gain in overall efficiency

Pre-duct

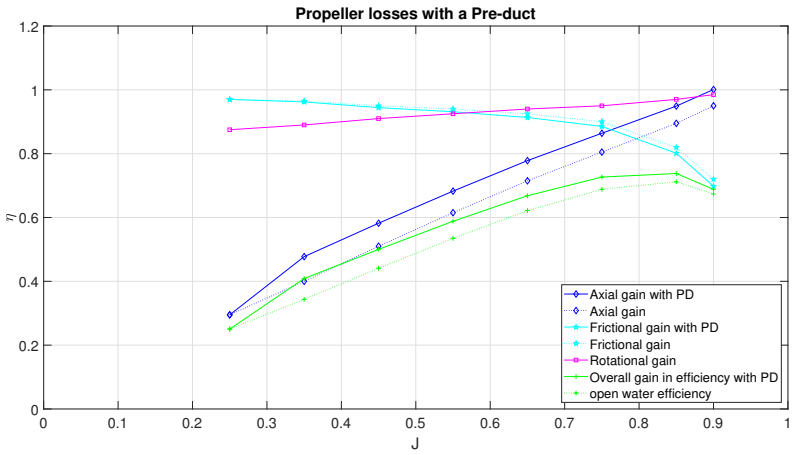

Figure 35: Influence of Pre-duct

A pre-duct leads to a decrease in axial kinetic energy losses. As mentioned before, the decrease in axial kinetic energy losses will be more at lower J values. Again, the efficiency gain has been calculated by taking the percentage decrease in the losses at each advance coefficient J from figure 25 and multiplying by gains decreasing linearly with advance coefficient J. Tables 12 and 13 show the decrease in axial and increase in frictional losses. Frictional losses are calculated in the same way as done for the pre-swirl stator. The axial losses are also calculated in a similar manner. The only difference is in the increase, or rather decrease in the gains in this case. This can be seen in table 14 where values in both the columns decrease as more savings will be obtained at lower J values. The gain at max J is taken as 5.4 and this is then linearly increased with decreasing J. The maximum gain is taken at lowest J can be seen in the second column 'Axial gain'. In figure 35, the blue line shows the decrease in axial losses when a pre-duct is used. The influence on frictional losses is represented by the cyan line and influence on rotational losses is assumed to be negligible. Table 15 shows the efficiency of the propulsor (propeller and pre-duct) which is denoted by η_{pd}. η_{pd} is calculated by using the formula : $\eta_{pd} = \eta_{apd}.\eta_r.\eta_{fpd}$

AXL	$\frac{1-AXL}{100}(\%)$	f_{esd}	$\eta_{a_{pd}}$
0.105	0.00895	0.077328	0.477328
0.11	0.0089	0.07209	0.58209
0.105	0.00895	0.067662	0.682662
0.1	0.009	0.06318	0.77818
0.09	0.0091	0.058968	0.863968
0.09	0.0091	0.054054	0.949054
0.055	0.00945	0.05103	1.00103

Table 12: Decrease in axial losses due to preduct

FricL	$\frac{1-FricL}{100}(\%)$	f_{esd}	$\eta_{f_{pd}}$
-0.005	0.01005	-0.00287	0.962129
-0.015	0.01015	-0.0058	0.9442
-0.01	0.0101	-0.00866	0.931343
-0.015	0.01015	-0.0116	0.9134
-0.025	0.01025	-0.01464	0.885357
-0.08	0.0108	-0.01851	0.801486
-0.1	0.011	-0.022	0.698

Table 13: Increase in frictional losses due to Pre-duct

J	Axial gain (%)	Fric div (%)
0.35	8.64	-0.28571
0.45	8.1	-0.57143
0.55	7.56	-0.85714
0.65	7.02	-1.14286
0.75	6.48	-1.42857
0.85	5.94	-1.71429
0.9	5.4	-2

Table 14: Gains applied on a Pre-duct

η_o	η_{pd}	η_{o_+}	η_{o_-}
0.250381	0.250381	0.260497	0.240466
0.34354	0.408733	0.425246	0.392547
0.440895	0.500145	0.52035	0.480339
0.534743	0.588108	0.611868	0.564819
0.621693	0.668142	0.695135	0.641684
0.688275	0.726674	0.756032	0.697898
0.711883	0.737834	0.767642	0.708615
0.67374	0.688238	0.716043	0.660984

Table 15: Gain in overall efficiency with a Preduct

Mewis duct

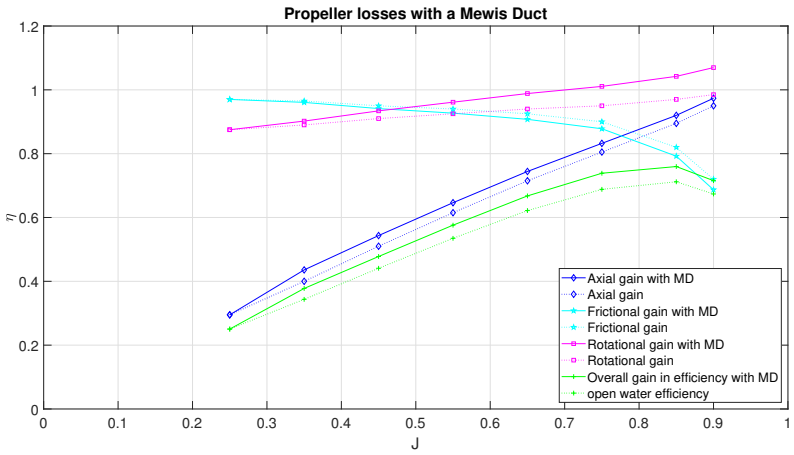

Figure 36: Influence of Mewis Duct

A Mewis duct can be thought of as a combination of pre-swirl and pre-duct and influences rotational, axial and frictional losses. Tables 16 and 17 show the decrease in rotational and axial losses. Table 18 shows the increase in frictional losses. The decrease in losses has been calculated in the same way as described for the pre-swirl stator and pre-duct for the respective losses. Table 19 shows the rotational gain, frictional loss and the axial gain. The frictional loss is taken as 3% at max J as a mewis duct has more surface area than a pre-duct or pre-swirl stator. It is also assumed that the ESD will have more of an influence on rotational losses than axial losses. Table 20 shows the gain in overall efficiency with a Mewis duct.

RotL	$\frac{1-RotL}{100}$ (%)	f_{esd}	$\eta_{a_{md}}$
0.015	0.00985	0.012101	0.902101
0.02	0.0098	0.02408	0.93408
0.015	0.00985	0.036304	0.961304
0.015	0.00985	0.048406	0.988406
0.01	0.0099	0.060814	1.010814
0.02	0.0098	0.07224	1.04224
0.015	0.00985	0.08471	1.06971

Table 16: Decrease in rotational losses due to Mewis duct

AXL	$\frac{1-AXL}{100}$ (%)	f_{esd}	$\eta_{a_{md}}$
0.105	0.00895	0.0358	0.4358
0.11	0.0089	0.033375	0.543375
0.105	0.00895	0.031325	0.646325
0.1	0.009	0.02925	0.74425
0.09	0.0091	0.0273	0.8323
0.09	0.0091	0.025025	0.920025
0.055	0.00945	0.023625	0.973625

Table 17: Decrease in axial losses due to Mewis duct

FricL	$\frac{1-FricL}{100}$ (%)	f_{esd}	$\eta_{f_{md}}$
-0.005	0.01005	-0.00431	0.960693
-0.015	0.01015	-0.0087	0.9413
-0.01	0.0101	-0.01299	0.927014
-0.015	0.01015	-0.0174	0.9076
-0.025	0.01025	-0.02196	0.878036
-0.08	0.0108	-0.02777	0.792229
-0.1	0.011	-0.033	0.687

Table 18: Increase in frictional losses due to Mewis duct

J	Rot. gain (%)	Fric loss (%)	Axial gain (%)
0.35	1.228571	-0.42857	4
0.45	2.457143	-0.85714	3.75
0.55	3.685714	-1.28571	3.5
0.65	4.914286	-1.71429	3.25
0.75	6.142857	-2.14286	3
0.85	7.371429	-2.57143	2.75
0.9	8.6	-3	2.5

Table 19: Gains applied on a Mewis duct

η_o	η_{md}	η_{o_+}	η_{o_-}
0.250381	0.250381	0.265707	0.235657
0.34354	0.377683	0.4008	0.355472
0.440895	0.477762	0.507005	0.449666
0.534743	0.575968	0.611222	0.542096
0.621693	0.66765	0.708515	0.628386
0.688275	0.738692	0.783906	0.695251
0.711883	0.759658	0.806155	0.714984
0.67374	0.715508	0.759303	0.67343

Table 20: Gain in overall efficiency with a Mewis duct

4.1 Sensitivity Analysis

Sensitivity analysis is shown for all the energy saving devices in figures 37, 38 and 39 where a deviation of $+/-2\%$ from the efficiency of the propulsor (propeller and ESD) is considered. These efficiencies can be seen

in the last two columns of tables 11, 15 and 20 for a pre-swirl stator, pre-duct and a mewis duct respectively. Here, η_{o_+} indicates deviation of +2% from the average savings while η_{o_-} indicates deviation of -2% from the average savings. A linear approach is a good approximation to predict the performance of these devices for a range of speeds, however, all devices need to be tailored to a specific ship and may not necessarily follow a linear energy saving pattern. Although, it is expected that the energy saving will lie somewhere between the range shown in these figures as the standard deviation of model tests and CFD simulations by different authors is 2%.

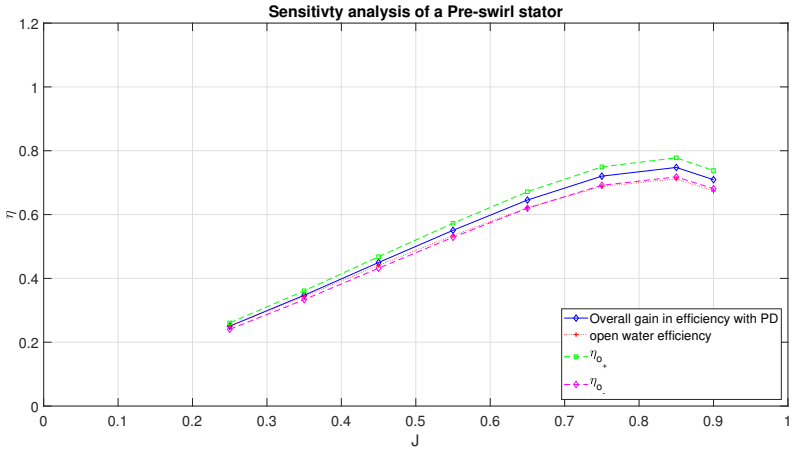

Figure 37: Sensitivity analysis of a Pre-swirl stator

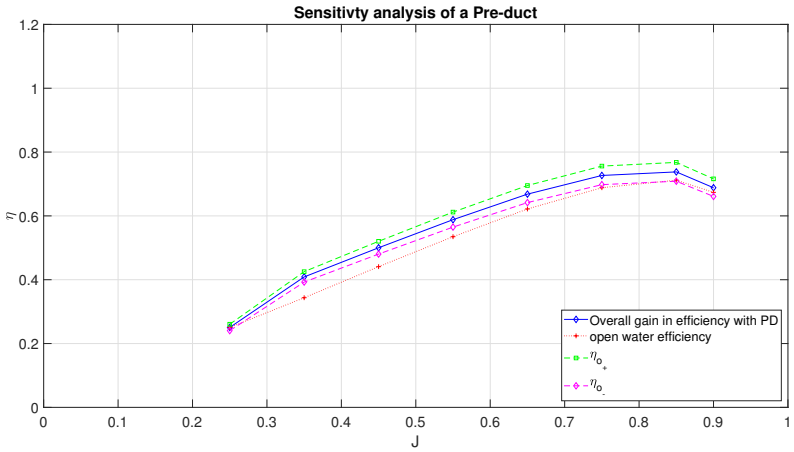

Figure 38: Sensitivity analysis of Pre-duct

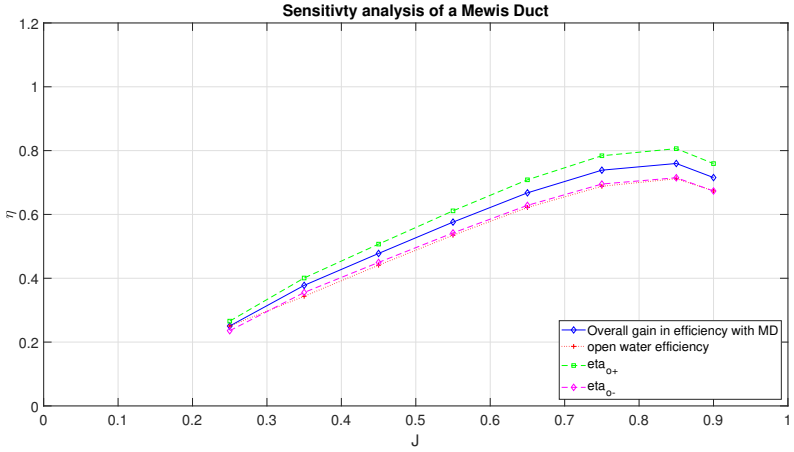

Figure 39: Influence of Mewis duct

5 Case Study

The model described in section 4 is implemented on a Chemical tanker *Castillo De Tebra*.

Figure 40: *Castillo De Tebra*

The vessel details and particulars can be seen in the table 21 and 22 respectively.

Ship Name	Castillo De Tebra
Class	BV
Ship Type	Tanker
Shipbuilder	Xinle Shipbuilding

Table 21: General Information

Length Between Perp.	L_{PP}	113.80 m
Breadth	B	22 m
Depth	H	11.40 m
Design Draft	T	8.50 m
Design Displacement	Δ_D	16988 m^3
Design Speed	V_D	13.27 kn
Power for propulsion		2919 kW @75% MCR

Table 22: Vessel Particulars

The main engine and propeller data is shown in tables 23 and 24 respectively.

Manufacturer	CSSC Marine Power
Type	6S35ME-B9.5
Maximum Continuous Rating (MCR)	4170kW @167 rpm
SFC at 75% MCR (g/kWh)	172.02
Fuel	Diesel Oil

Table 23: Main Engine Data

Type	CPP
Blades	4
Diameter	4.3 m
Speed	167 rpm

Table 24: Propeller Data

To apply the model described in section 4, test data for all ship speeds is required. However, the test data is available only for a higher speed range 11.5 - 15 knots. Therefore, a model proposed by de Vos et al. [34] is reproduced to obtain data for all speeds. In their model, a few variables have been normalised by relating the variables of off-design condition to the corresponding variables of a known nominal conditions. Normalisation is done using the equation 17

$$X^* = \frac{X}{X_{nom}} \tag{17}$$

where X^* is the normalised variable, X_{nom} is the corresponding nominal value of the variable and X is the relevant variable to be normalised.

The variables which have been normalised are the specific resistance C_E, propeller thrust coefficient K_T, propeller torque coefficient K_Q, wake fraction w, thrust deduction factor t and the relative rotative efficiency η_R.

Specific Resistance

$$C_E^* = \underbrace{\underbrace{1 - a_{CE}}_{\text{Basic viscous resistance}} + \underbrace{k_{CE}\left(v_s^* - 1\right)}_{\text{Linear correction viscous resistance}} + \underbrace{c_{CE} \cdot \left(e^{d_{CE} \cdot v_s^*} - e^{d_{CE}}\right)}_{\text{Non-linear correction viscous resistance}}}_{\text{Viscous resistance}} + \underbrace{a_{CE} \cdot e^{b_{CE} \cdot (v_s^* - 1)}}_{\text{Wavemaking resistance}} \tag{18}$$

Thrust and Torque coefficient

$$K_T{}^* = 1 + a_{prop}(J^* - 1) + c_{prop}(J^* - 1)^2 \tag{19}$$

$$K_Q{}^* = 1 + b_{prop}(J^* - 1) + d_{prop}(J^* - 1)^2 \tag{20}$$

Wake fraction, thrust deduction factor and relative rotative efficiency

$$w^* = 1 - c_w(1 - v_s{}^*) + d_w(1 - v_s{}^*)^2 \tag{21}$$

$$t^* = 1 - c_t(1 - {v_s}^*) + d_t(1 - {v_s}^*)^2 \tag{22}$$

$${\eta_R}^* = 1 - c_{\eta_R}(1 - {v_s}^*) + d_{\eta_R}(1 - {v_s}^*)^2 \tag{23}$$

Mechanical transmission losses

$${M_{loss}}^* = k_a {M_{in}}^* + k_b {N_{in}}^* + k_c \tag{24}$$

where k_a is the coefficient related to the torque, k_b is the coefficient related to the rotational speed and k_c is the coefficient related to constant torque loss. The coefficient of shaft-line losses are set as: $k_a = 0.7$, $k_b = 0.3$, $k_c = 0$ and the nominal shaft efficiency is set as 0.99. Having said this, the transmission efficiency η_{TRM} is taken as 0.99 as it hardly changes for all speeds[34].

Calculations

The coefficients of the above equations are shown in appendix A. C_E is calculated from equation 18 and c1 is calculated from C_E as :

$$c1 = C_E.\rho^{\frac{1}{3}}.\Delta^{\frac{2}{3}}.{v_S}^3 \tag{25}$$

where ρ is the density of water and Δ is the displacement volume $17233.561m^3$.
The effective towing power P_E is calculated by :

$$P_E = c1.{v_S}^3 \tag{26}$$

The resistance R is calculated from P_E :

$$R = \frac{P_E}{v_s} \tag{27}$$

The wake fraction w and thrust deduction factor is calculated using equations 21 and 22. And thrust and torque coefficients, K_T and K_Q, are calculated using equations 19 amd 20. The open water efficiency is then calculated by :

$$\eta_o = \frac{1}{2\pi}\frac{K_T}{K_Q}J \tag{28}$$

It is assumed that the propeller of *Castillo De Tebra* has similar axial, rotational and frictional losses as that of the propeller seen in figure 25 in section 1.4. Thus, the axial, rotational and frictional efficiencies are calculated using regression analysis. A check is also performed using the equation 16 described by Molland et. al[5]. This can be seen in table 31 in appendix B. Both 'η_o' and 'η_o check' are highlighted in green.
c7 or $\frac{k_T}{J^2}$ is then calculated by :

$$c7 = \frac{R}{(1-t).(1-w)^2.\rho.{v_s}^2.D^2} \tag{29}$$

The values of J w.r.t to the ship speed (1-15 knots) are determined using regression analysis as c7 is available from the open water diagram as well. Since there is no gearbox, the propeller and engine rpm are the same. A relation between ship and propeller rpm can now be found with :

$$J = \frac{v_A}{n.D} \tag{30}$$

where D is the diameter of the propeller - 4.3m, and v_A is advance velocity and is defined by $v_A = v_S(1 - w)$. The hull efficiency can be found out from :

$$\eta_H = \frac{1-t}{1-w} \tag{31}$$

Now, the propulsive efficiency of the propeller is determined using:

$$\eta_D = \eta_H . \eta_R . \eta_o \tag{32}$$

The delivered power P_D is the same as the propeller power P_p as there is only one propeller installed on the vessel. It can be determined by :

$$P_D = \frac{P_E}{\eta_D} \tag{33}$$

A relation between shaft power P_S and delivered power P_D is available from the shipyard where the vessel was built. This helped is determining the shaft power. As mentioned earlier, the transmission efficiency η_{TRM} is taken as 0.99 for all speeds. The brake power P_B is then determined by :

$$P_B = \frac{P_S}{\eta_{TRM}} \tag{34}$$

The results of the above calculations can be seen in appendix B in table 31 and appendix C in tables 32, 33 and 34.

EEDI

The Energy Efficiency Design Index (EEDI) is a measure of ship's energy efficiency ($\frac{g}{t}nm$) and is calculated by the following formula :

$$\begin{aligned}
&\frac{1}{f_i \cdot f_c \cdot f_l \cdot Capacity \cdot f_w \cdot V_{ref}} \\
&\cdot \left[\left(\prod_{j=1}^{n} f_j \right) \left(\sum_{i=1}^{n_{ME}} P_{ME(i)} \cdot C_{FME(i)} \cdot SFC_{ME(i)} \right) \right. \\
&\quad + (P_{AE} \cdot C_{FAE} \cdot SFC_{AE}) \\
&\quad + \left(\left(\prod_{j=1}^{n} f_j \cdot \sum_{i=1}^{n_{PTI}} P_{PTI(i)} - \sum_{i=1}^{n_{eff}} f_{eff(i)} \cdot P_{AEeff(i)} \right) C_{FAE} \cdot SFC_{AE} \right) \\
&\quad \left. - \left(\sum_{i=1}^{n_{eff}} f_{eff(i)} \cdot P_{eff(i)} \cdot C_{FME} \cdot SFC_{ME} \right) \right]
\end{aligned} \tag{35}$$

where

P_{ME}: Main Engine Power (kW) = 2919;

P_{AE}: Auxiliary Engine Power (kW) =208.5;

SFC: Specific fuel consumption (g/kW) = 172.02(ME) , 230 (AE);

C: Fuel to CO_2 factor (g CO_2/g Fuel)= 3.206;

Capacity: for Cargo ships DWT = 13021.1;

V_{ref}: Reference speed (knots)= 14;

f_c: Correction factor for capacity = 1.0;

f_w: Correction factor for performance in real weather = 1.0 ;

f_i: Correction factor for efficiency = 1.027.

The values for the above coefficient and variables have been taken from the Sea trial report which was provided by the shipyard.

6 Results

In this chapter, the results obtained after implementing the model described in chapter 4 on *Castillo De Tebra*, will be discussed.

6.1 Propeller Loss Diagrams

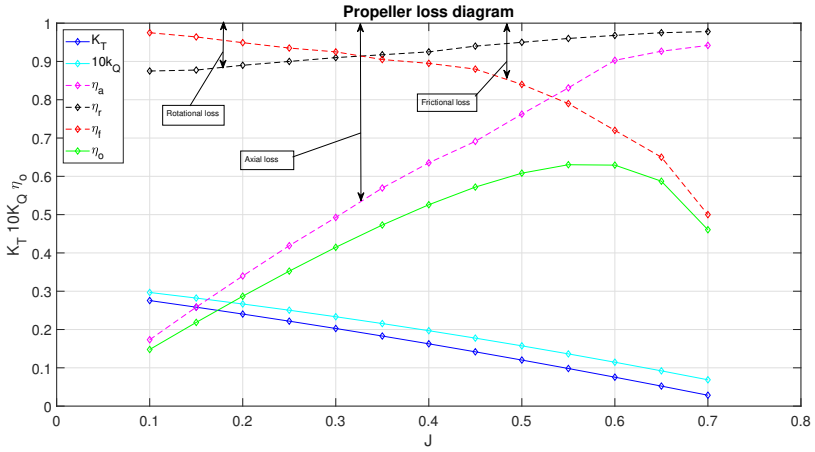

Figure 41: Propeller loss diagram of *Castillo De Tebra*

As mentioned earlier, it is assumed that the propeller loss diagram of *Castillo De Tebra* has similar axial, rotational and frictional losses as that of the propeller seen in figure 25. Figure 41 shows the different kinds of losses associated with the propeller of the tanker. The model described in chapter 4 is applied to this propeller.

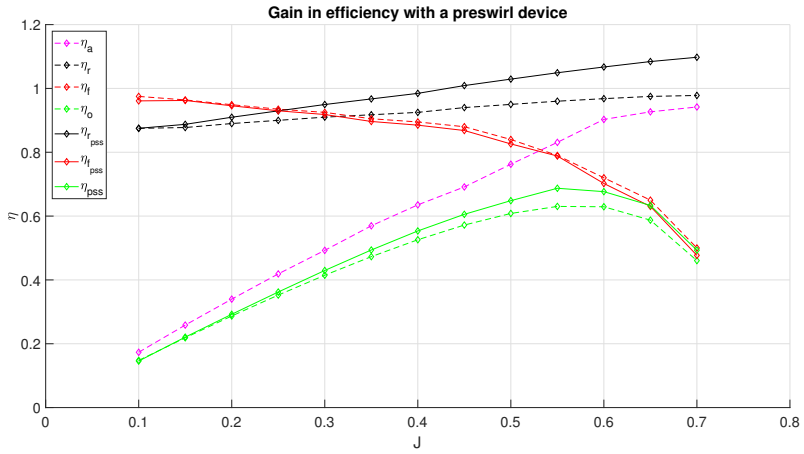

Figure 42: Propeller loss diagram of *Castillo De Tebra* with a Pre-swirl stator

Figure 42 shows the influence of a Pre-swirl stator on rotational and frictional losses. An increase in rotational efficiency with increasing advance coefficient J is seen whereas the frictional efficiency decreases with increasing J. Hence, the frictional efficiency is lower than what it would be without the ESD. The method to calculate the influence of a Pre-swirl stator on the rotational and frictional efficiencies has been described in detail in chapter 4. In appendix D.1, table 35 shows the decrease in rotational losses with a Pre-swirl stator, table 36 shows the increase in frictional losses with a Pre-swirl stator. Table 37 shows the energy saving factor used which is the same as described in chapter 4.

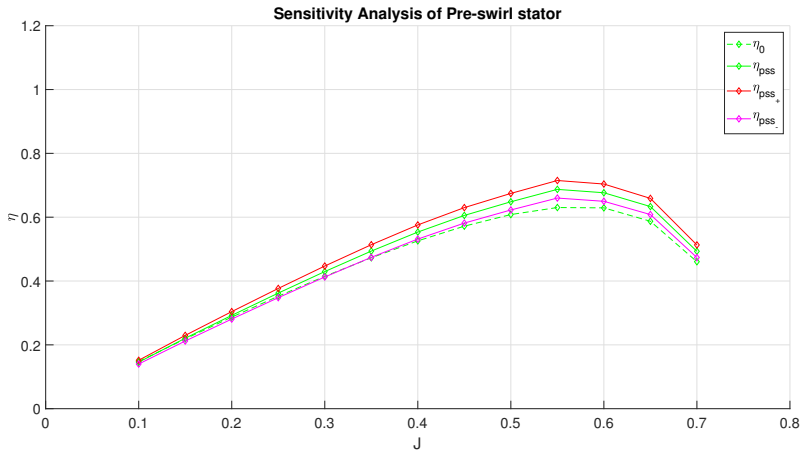

Figure 43: Sensitivity analysis of gain in propulsive efficiency with a Pre-swirl stator

Figure 43 shows the gain efficiency with and without a Pre-swirl stator. η_{o_+} depicts the efficiency with a deviation of +2% gain in axial and frictional efficiency and η_{o_-} depicts the efficiency with a deviation of -2% gain in axial and frictional efficiency. Table 38 in appendix D.1 shows the calculated values of these efficiencies.

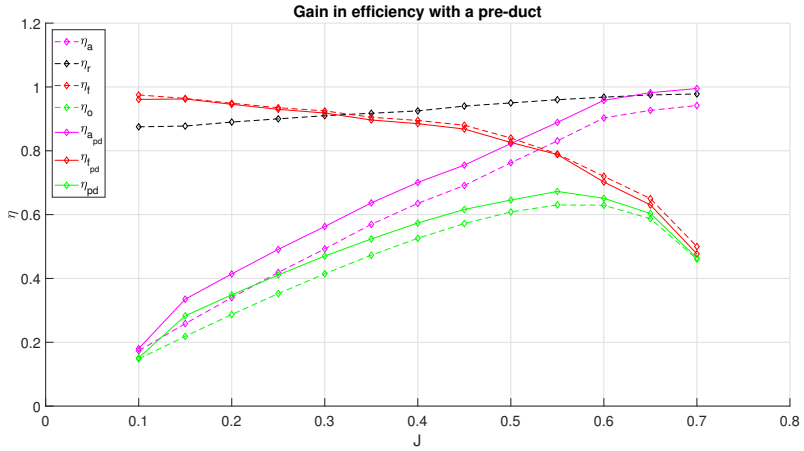

Figure 44: Propeller loss diagram of *Castillo De Tebra* with a Pre-duct

Figure 44 shows the influence of a Pre-duct on axial and frictional losses. An increase in axial efficiency is seen at lower advance coefficient values and this gradually decreases with increase in J whereas the frictional efficiency decreases with increasing J. Hence, the frictional efficiency is lower than what it would be without the ESD. The method to calculate the influence of a pre-duct on the axial and frictional efficiencies has been described in detail in chapter 4. In appendix D.2, table 39 shows the decrease in axial losses with a Pre-duct, table 40 shows the increase in frictional losses with a Pre-duct. Table 41 shows the energy saving factor used which is the same as described in chapter 4.

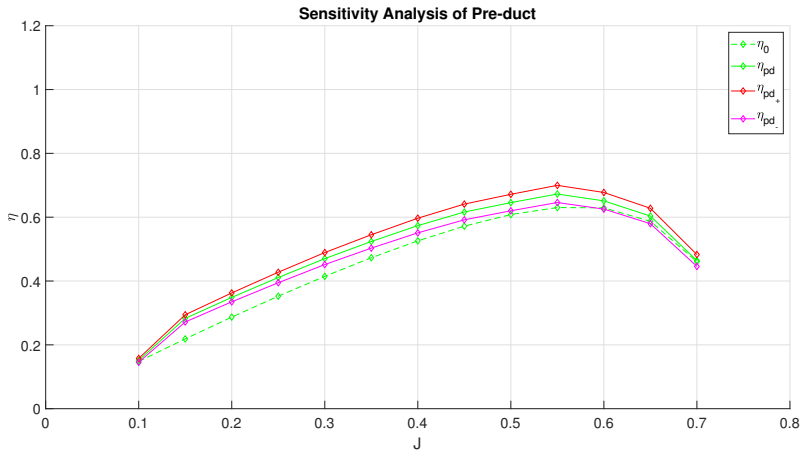

Figure 45: Sensitivity analysis of gain in propulsive efficiency with a Pre-duct

Figure 45 shows the gain in efficiency with and without a Pre-duct. η_{o_+} depicts the efficiency with a deviation of +2% gain in axial and frictional efficiency and η_{o_-} depicts the efficiency with a deviation of -2% gain in axial and frictional efficiency. Table 42 in appendix D.2 shows the calculated values of these efficiencies.

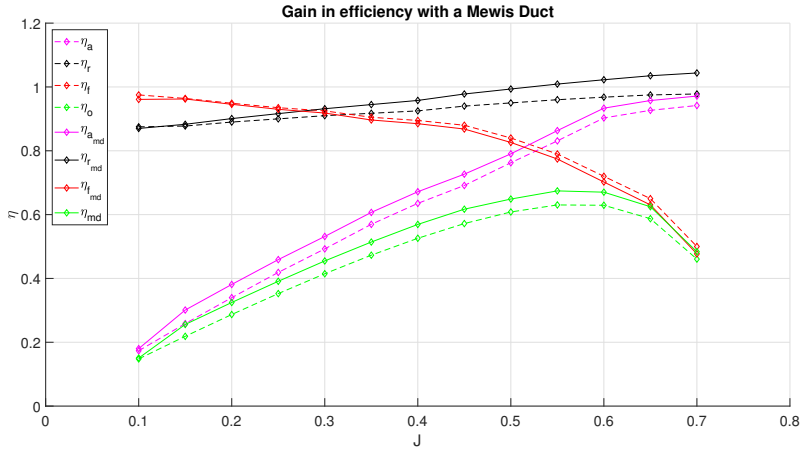

Figure 46: Propeller loss diagram of *Castillo De Tebra* with a Mewis duct

Figure 46 shows the influence of a Mewis duct on axial, rotational and frictional losses. An increase in axial efficiency is seen at lower advance coefficient values and this gradually decreases with increase in J. Also, an increasing in rotational efficiency is seen with increasing J whereas the frictional efficiency decreases with increasing J. Hence, the frictional efficiency is lower than what it would be without the ESD. The method to calculate the influence of a pre-duct on the axial and frictional efficiencies has been described in detail in chapter 4. In appendix D.3, table 44 shows the decrease in axial losses with a Mewis duct, table 43 shows the decrease in rotational losses with a Mewis duct, table 45 shows the increase in frictional losses with a Mewis duct. Table 43 shows the energy saving factor used which is the same as described in chapter 4.

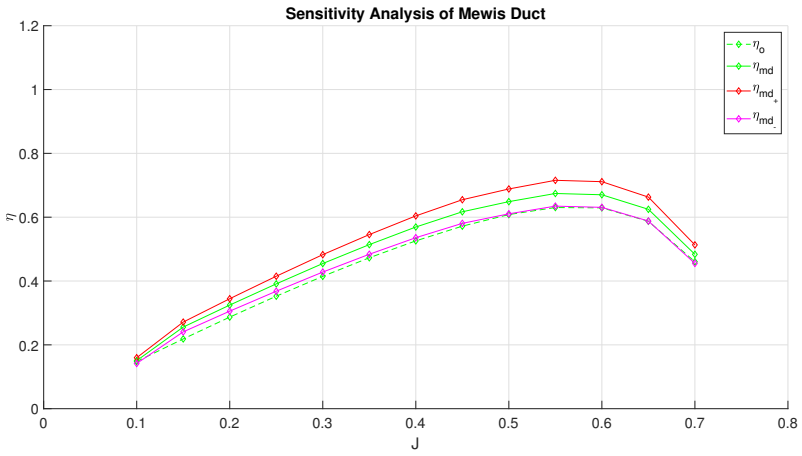

Figure 47: Sensitivity analysis of gain in propulsive efficiency with a Mewis duct

Figure 47 shows the gain in efficiency with and without a Mewis duct. η_{o_+} depicts the efficiency with a deviation of +2% gain in axial and frictional efficiency and η_{o_-} depicts the efficiency with a deviation of -2% gain in axial and frictional efficiency. Table 47 in appendix D.3 shows the calculated values of these efficiencies.

6.2 Engine Envelope

The engine envelope of *Castillo De Tebra* with the application of the three ESDs is shown in figures 48, 49 and 50 respectively. The sensitivity analysis of +/-2% from average power savings is shown in the envelope. The calculated values for the three ESDs are shown in appendix E in tables 48, 49 and 50 respectively. The blue line in the engine envelope indicates the brake power of the engine without the ESD. The green line indicates the brake power with the ESD, The magenta and the black line indicate the brake power with a deviation of +2% and -2% in power savings respectively. The black dotted line indicates 75% MCR and the two cyan line represent the upper and lower speed limit. The upper speed limit is present because speeds above that can damage the rotating and translating parts of the engine like crankshaft, piston and piston rods. The lower speed limit is present as below this speed limit, the engine does not run smoothly and may even stop running altogether. This is caused by failure of ignition due to lack of compression[31].

The red line represents the power limit. The power is limited by the maximum fuel injected per cycle. If the efficiency is assumed to be constant, this curve is ideally a straight line through the origin of the power speed curve[31]. The reduction in power demand can be clearly seen for the three upstream ESDs. The reduction in power is prominent at higher speeds and marginal at low-medium speeds.

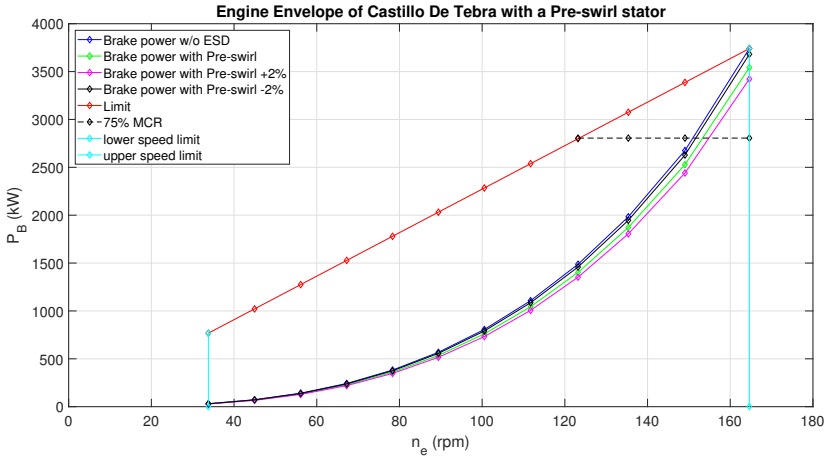

Figure 48: Engine envelope with a Pre-swirl stator

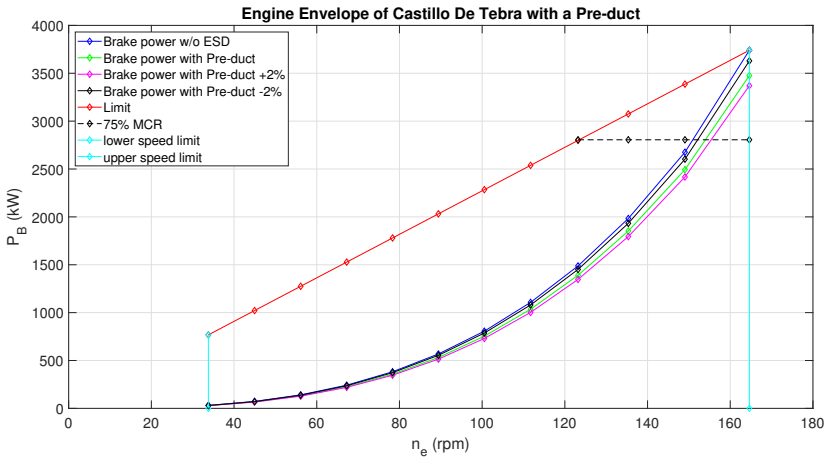

Figure 49: Engine envelope with a Pre-duct

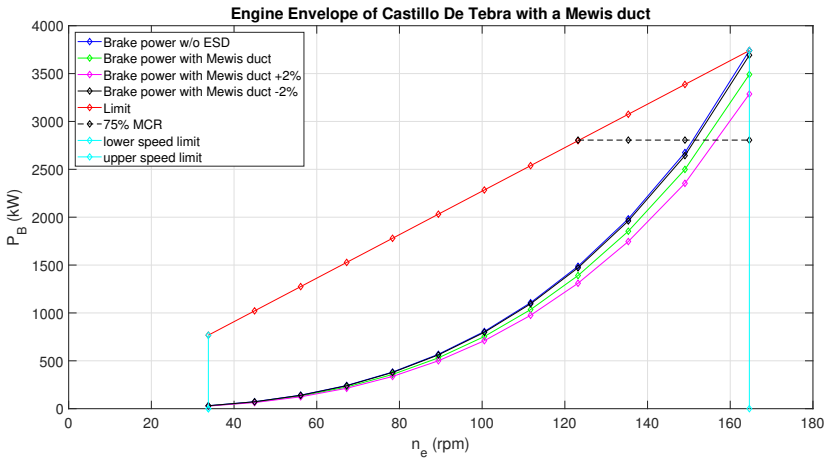

Figure 50: Engine envelope with a Mewis duct

6.3 Analysis and Interpretation

In this section, the power savings by the three ESDs with respect to ship speed will be compared for three different cases:

1. Average power gains obtained by the three ESDs, shown in figure 51.
2. Average gains with +2% deviation in power savings obtained by the three ESDs, shown in figure 52.
3. Average gains with -2% deviation in power savings obtained by the three ESDs, shown in figure 53.

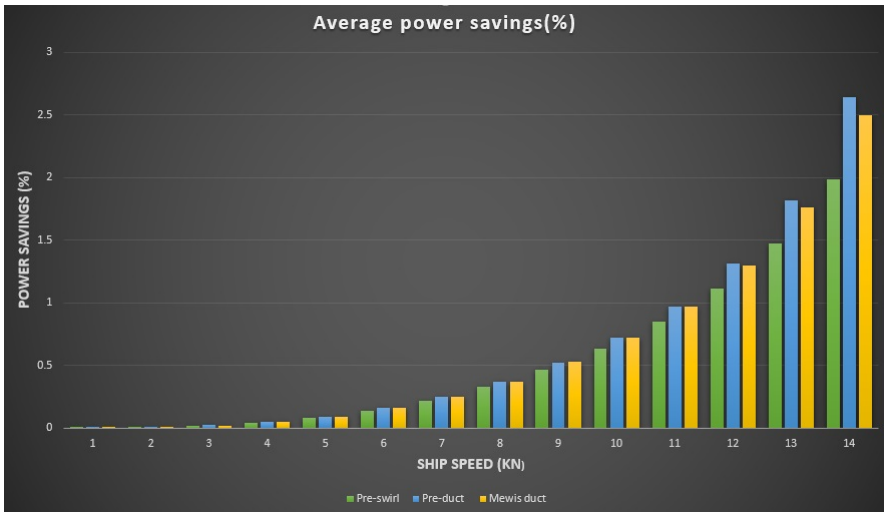

Figure 51: Average powers savings w.r.t ship speed

The model yields highest average power savings for a Pre-duct. This can be seen in figure 51.

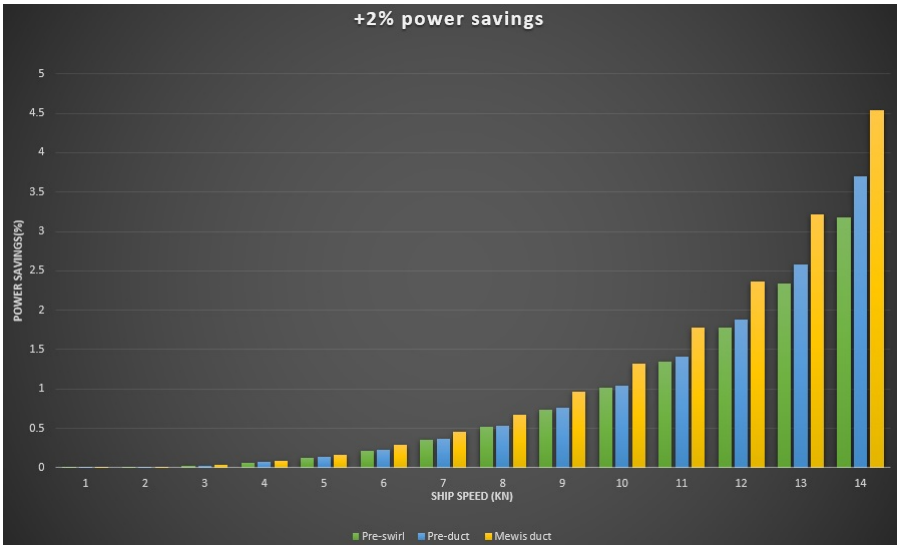

Figure 52: Average powers savings with a deviation of +2% w.r.t ship speed

It is seen in figure 52 that the average power savings with a deviation of +2% is the highest for a Mewis duct.

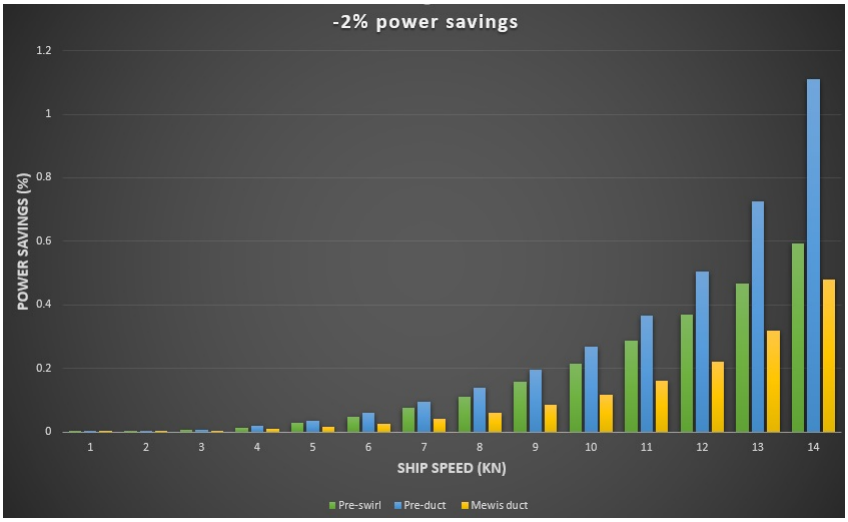

Figure 53: Average powers savings with a deviation of -2% w.r.t ship speed

The average power savings with a deviation of -2% is the highest for a Pre-duct. This is seen in figure 53.

One thing which is noticeable in the above figures is that the highest power savings are obtained for a Pre-duct for average power savings and power savings with a deviation of -2% from the average power savings. Mewis duct shows the highest power savings for power savings with a deviation of +2% from the average power savings. This supports the literature that the performance of these devices can be unpredictable. The sensitivity analysis was done to account for these uncertainties.

By looking at the above graphs, it can be stated that the performance of a Mewis duct is a bit more uncertain when compared to the other two ESDs. This could be due to interaction effects that take place when a Mewis duct is installed on a vessel. A Mews duct, as mentioned earlier, has an influence all three (axial, rotational and frictional) losses. So, the stator fins which have an influence on the rotational losses, may interfere with the flow regime on which the duct works on. The duct is there to reduce axial losses but there can be interaction

effects which can lead to unpredictable outcomes.

Verfication

The model described in chapter 4 is verified by a study conducted by Mewis[29]. This can be seen in figure 54 .The power savings of *Castillo De Tebra* for a mewis duct was found to be 4.5% at a deviation of +2% from average power savings at design speed. This fits in well with the model tests performed by Friedrich Mewis on various kinds of vessels.

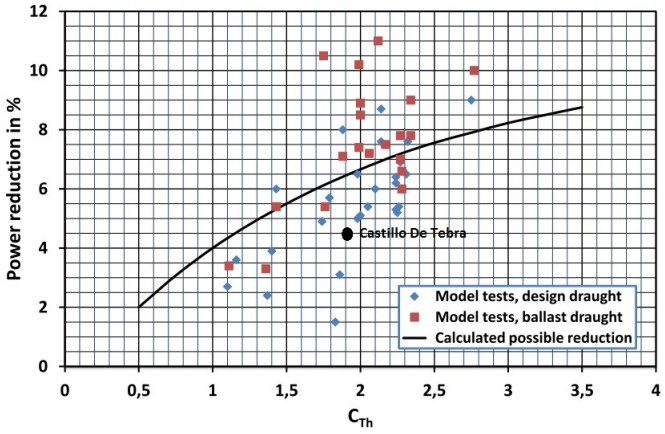

Figure 54: Power reduction by Mewis Duct - Model test results

EEDI

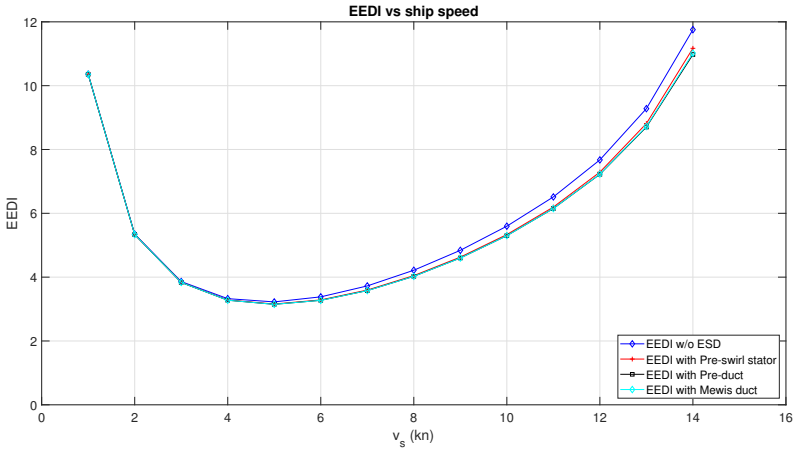

Figure 55: Comparison of EEDI by the ESDs

The difference in EEDI with and without ESDs can be clearly seen in figure 55. There is a reduction in EEDI when the ESDs are used and this reduction is prominent, especially, at higher speeds. The EEDI is calculated using equation 35 and the calculated values are shown in appendix F in table 51.

6.4 Gain in propulsive efficiency

In this section, the average gain in propulsive efficiency with the three ESDs is shown w.r.t to the ship speed and advance coefficient J.

Pre-swirl Stator

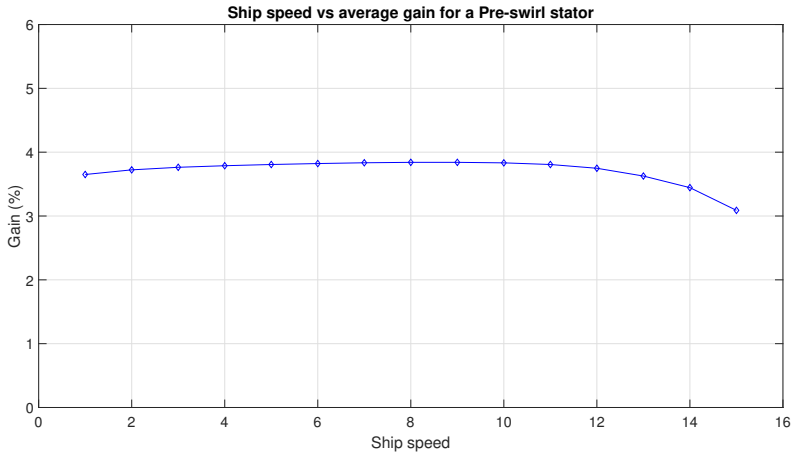

Figure 56: Gain in propulsive efficiency w.r.t ship speed

As seen in figure 56,the gain is between 3-4% for all speeds. A slight increase in gain is shown till 10 knots and then the gain starts decreasing gradually.

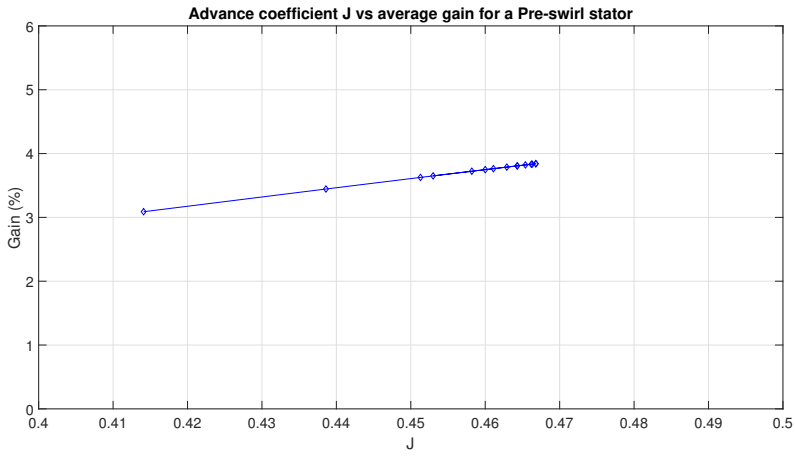

Figure 57: Gain in propulsive efficiency w.r.t Advance coefficient J

A linear increase of gain w.r.t J is yielded by the model for a Pre-swirl stator, which is not surprising considering the linear approach taken to build the model. This can be seen in figure 57.

Pre-duct

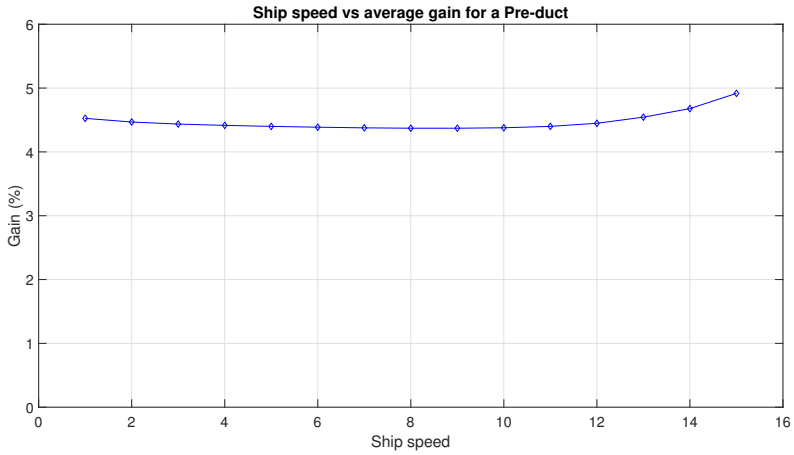

Figure 58: Gain in propulsive efficiency w.r.t ship speed

A very slight decrease of gain w.r.t to speed is observed till 8 knots and then a gradual increase is seen. This is depicted by figure 58.

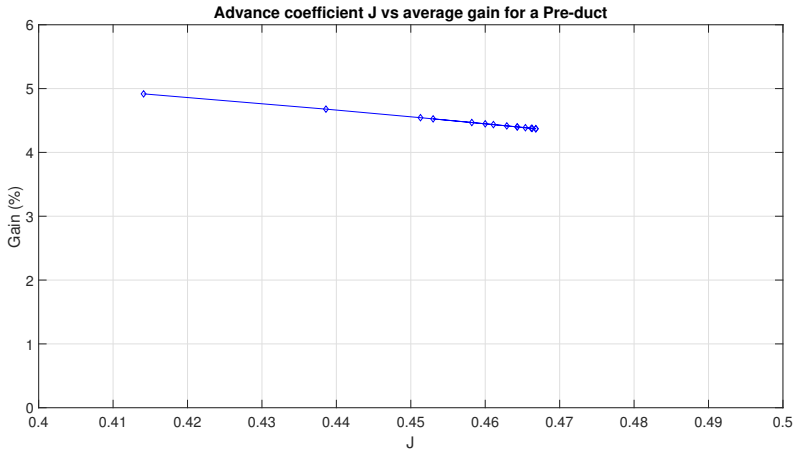

Figure 59: Gain in propulsive efficiency w.r.t Advance coefficient J

In figure 59, a linear decrease of gain is seen w.r.t J as higher gains at expected at lower speeds for a Pre-duct. This is explained in chapter 4.

Mewis duct

The gain in efficiency for a Mewis duct is almost constant as seen in figures 60 and 61. This is understandable as mewis duct influences the frictional, rotational and axial losses associated with the propeller. The rotational losses decreases linearly with J whereas the axial losses increases linearly with J as explained in chapter 4.

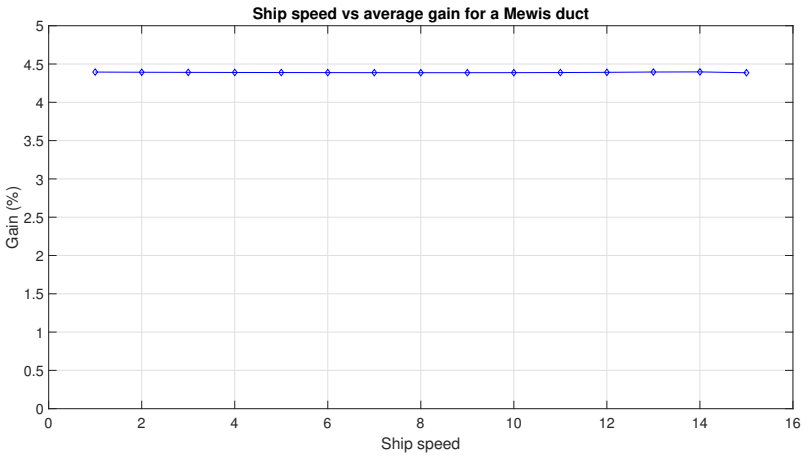

Figure 60: Gain in propulsive efficiency w.r.t ship speed

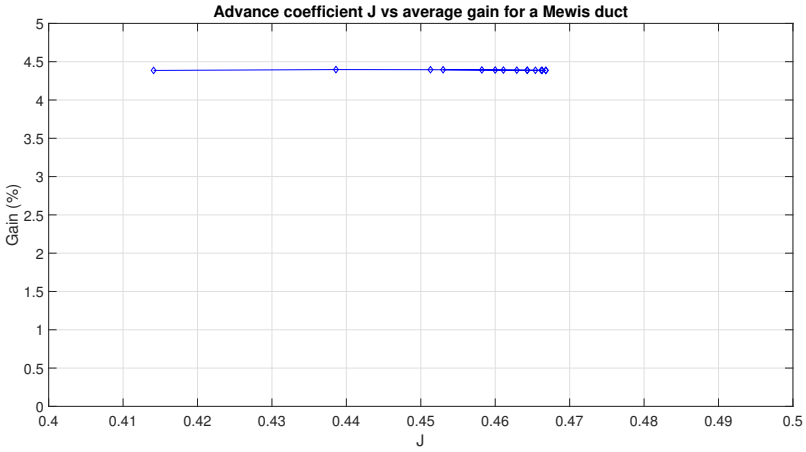

Figure 61: Gain in propulsive efficiency w.r.t Advance coefficient J

6.5 Limitations of the model

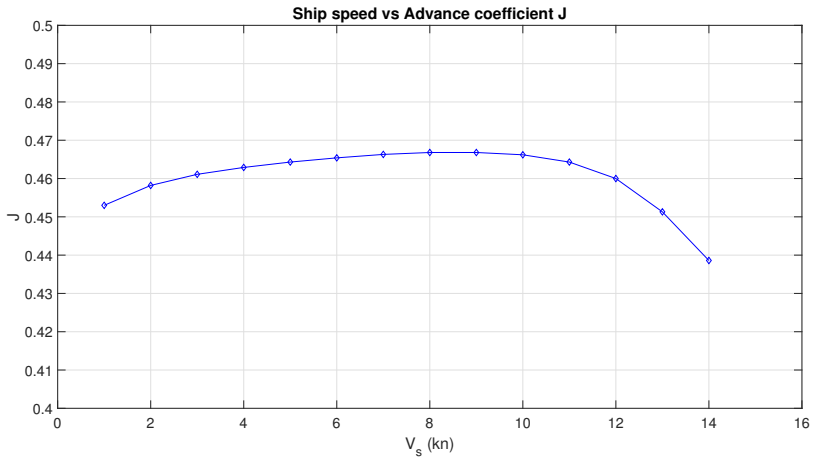

Figure 62: Advance coefficient J vs Ship speed

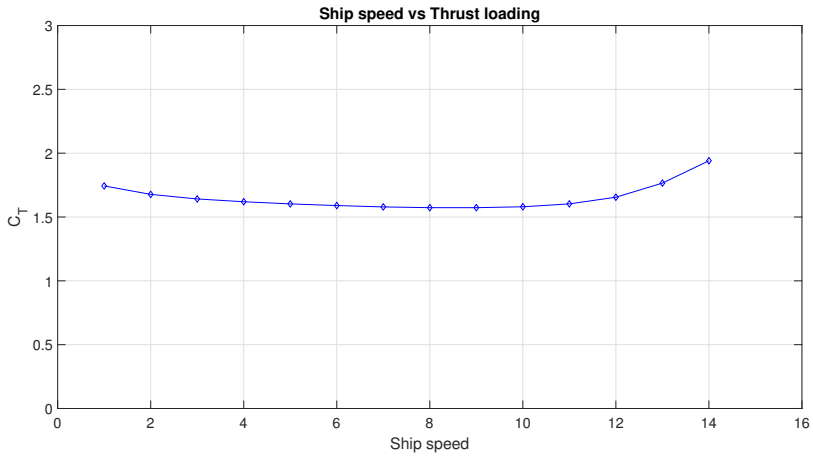

Figure 63: Thrust loading C_T vs Ship speed

- The model is not validated. The model can be validated only by performing model tests (towing tank) or by performing CFD simulations at different speeds. This could not be done due to the time constraint and complexity of the required tests.
- The model does not take into account that the energy saving effect could also be non-linear with respect to the advance coefficient.

  The following is not exactly a limitation but something that should be mentioned. The model described in chapter 4 is based on the J values from 0-0.7, whereas it is noticed from the calculations that the ship speed range lies between J values of 0.43 and 0.47. So the efficiency gain with respect to the ship does not really change much. The postulation is based on a linear approach towards increase in energy savings with respect to the advance coefficient. Although, J does increase with the ship speed for the most part of the speed range, the increase is very gradual. Power savings are seen mostly for medium and high speed ranges for the tanker i.e in the range of 8-14 knots and this is caused more due to the specific resistance C_E of the vessel and not due to energy saving from the ESDs as the energy gains for all ESDs remain somewhat similar for all ship speeds.

7 Conclusion

The aim of the graduation project was to evaluate the effect of three upstream energy saving devices on engine operation. The three energy savings devices are Pre-swirl stator, Pre-duct and Mewis duct.
To evaluate the effect, a mathematical model described in chapter 4 is proposed. This model adopts a linear approach towards energy saving effect with respect to the advance coefficient. Influence on energy losses depends on the type of energy saving device. The following conclusions are made based on the results obtained in chapter 6.

- The general perception until now was that ESDs act as a brake at lower speeds i.e they produce drag instead of thrust at lower speeds. But the results from the model do not agree with this. The energy saving remains more or less the same for all speeds, as seen in chapter 6 under section 6.4. This is because the advance coefficient is weakly dependent on ship speed and is almost constant for all ship speeds. This can be seen in figure 62.
- The energy saving depends on the thrust loading coefficient C_T and not solely on ship speed. With this being said, the thrust loading coefficient remains almost constant through all ship speeds (for this ship), so ideally, the energy saving for all ship speeds should also remain almost constant. This can seen is figure 63 in chapter 6 under subsection 6.5. Mewis[14] states that the energy saving of mewis duct depends on the propeller thrust coefficient C_T and ship speed.
- The power saving for Mewis duct for thrust loading C_T of around 1.9 is verified using figure 54 in chapter 6 under section 6.3.
- Power savings are seen for medium and higher speed ranges (> 10 knots). Savings at lower speeds are marginal and hardly noticeable. This is discussed in chapter 6 under subsection 6.3.
- The energy savings at lower speeds hardly matter as power savings are marginal.
- ESDs can help reduce the EEDI score as in seen in figure 55.
- ESDs may not be the answer to zero carbon emission vessels, but every step forward towards a greener environment must be considered as a positive step.

The conclusions mentioned above are made by answering the sub-questions mentioned in the objective 1.2 of this report.

1. The upstream ESDs or ESDs installed in front of the propeller are described in chapter 2 under section 2.2.1. For this project, performance of three upstream ESDs : Pre-duct, Pre-swril stator and Mewis duct is assessed.
2. The performance of upstream ESDs in design condition is presented in chapter 3 under table 3 and their performance in part-load conditions is discussed in the same chapter under section 3.1.
3. The performance of the aforementioned ESDs are modelled simplistically in chapter 4.
4. The effect these ESDs on the engine operation is discussed with help of a case study in chapter 6 under section 6.2. A reduction in power demand is prominent at higher speeds.
5. The effect these devices on EEDI for all ship speeds is presented in chapter 6 under section 6.3. A reduction in EEDI is seen, especially, at higher speeds.

8 Recommendations

The impact of ESDs on engine operation and EEDI in part-load condition has remained a question mark over the years. The model described in chapter 4 tries to capture the effect of three upstream ESDs on engine operation. However, the model has some limitations which have already been discussed in chapter 6 under section 6.5. Model tests or CFD simulations need to be performed to validate this model. It would be interesting to see if the losses, in fact, decrease linearly with increasing advance coefficient and if they lie within the range of the sensitivity analysis as shown in chapter 6 under section 6.1.

In this graduation project, a linear approach towards energy saving with respect to advance coefficient is modelled. A non-linear approach could also be considered here, although, this approach should only be considered if results from CFD simulations and model tests do not agree with the linear approach, as this approach would not be easy to model because there are too many types of non-linear equations and it would be hard to determine which one to use.

References

[1] J. H. de Jong. "A Framework for Energy Saving Device (ESD) Decision Making". In: *Ship Efficiency* (2011).

[2] Terwisga and Schuiling. "Hydrodynamic working principles of pre-ducts in ship propulsion". In: (2017).

[3] E. Korkut. "A case study for the effect of a flow improvement device (a partial wake equalizing duct) on ship powering characteristics". In: *Ocean Engineering* 33.2 (2006), pp. 205–218. ISSN: 00298018. DOI: 10.1016/j.oceaneng.2005.03.010.

[4] M. Organization. "Reducing CO 2 Emissions to Zero : The ' Paris Agreement for Shipping ' Implementing the Initial Strategy on Reduction of GHG Emissions from Ships (adopted by the UN International". In: ().

[5] T. H. Aria Molland. "Reducing ship emissions : A review of potential practical improvements in the propulsive efficiency of future ships REDUCING SHIP EMISSIONS : A REVIEW OF POTENTIAL PRACTICAL". In: April (2014). DOI: 10.3940/rina.ijme.2014.a2.289.

[6] K. J. Lee et al. "A performance study on the energy recovering turbine behind a marine propeller". In: *Ocean Engineering* 91 (2014), pp. 152–158. ISSN: 00298018. DOI: 10.1016/j.oceaneng.2014.09.004. URL: http://dx.doi.org/10.1016/j.oceaneng.2014.09.004.

[7] A. S. Olsen. "Energy coefficients for a propeller series". In: *Ocean Engineering* 31.3-4 (2004), pp. 401–416. ISSN: 00298018. DOI: 10.1016/j.oceaneng.2003.06.002.

[8] T. van Terwisga. "On the working principles of Energy Saving Devices". In: *3rd International Symposium on Marine Propulsors* May (2013), pp. 1–9.

[9] Carlton J. *Marine Propellers and Propulsion,3rd ed. Oxford: Butterworth-Heinemann; 2012.*

[10] J. G. Reyer Riemeijer. *Insight into Energy Saving Devices*. TU Delft. May 2018.

[11] J. H. Kim et al. "Development of Energy-Saving devices for a full Slow-Speed ship through improving propulsion performance". In: *International Journal of Naval Architecture and Ocean Engineering* 7.2 (2015), pp. 390–398. ISSN: 20926790. DOI: 10.1515/ijnaoe-2015-0027.

[12] H. J. Shin et al. "Numerical and experimental investigation of conventional and un-conventional preswirl duct for VLCC". In: *International Journal of Naval Architecture and Ocean Engineering* 5.3 (2013), pp. 414–430. ISSN: 20926790. DOI: 10.3744/JNAOE.2013.5.3.414.

[13] F. Mewis, T. Guiard, and S. Leonard. "The Becker Mewis Duct - Challenges in Full-Scale Design and new Developments for Fast Ships". In: *3rd International Symposium on Marine Propulsors* May (2013), pp. 519–527.

[14] F. Mewis. "A Novel Power-Saving Device for Full-Form Vessels". In: June (2009).

[15] X. Chang et al. "Investigation of the effects of a fan-shaped Mewis duct before a propeller on propulsion performance". In: *Journal of Marine Science and Technology (Japan)* 0.0 (2018), pp. 1–14. ISSN: 09484280. DOI: 10.1007/s00773-018-0530-x. URL: http://dx.doi.org/10.1007/s00773-018-0530-x.

[16] F. Çelik. "A numerical study for effectiveness of a wake equalizing duct". In: *Ocean Engineering* 34.16 (2007), pp. 2138–2145. ISSN: 00298018. DOI: 10.1016/j.oceaneng.2007.04.006.

[17] Z. Soek Lee and Shigunov. "Design and Performance Analysis of vane wheel". In: 64.19 (2016), pp. 5000–5010.

[18] marinewiki. *Vane Wheels*. URL: http://marinewiki.org/index.php/Vane_Wheels (visited on 12/11/2018).

[19] L. Xia, J. Lundberg, and R. E. Bensow. "Performance Prediction of a Nozzle Propeller". In: *Proceedings of the 29th Symposium on Naval Hydrodynamics* 1.August (2012), pp. 26–31.

[20] T. Dalgleish et al. "A Study on the propulsive performance of Hi-Fin ". In: *Journal of Experimental Psychology: General* 136.1 (2007), pp. 23–42.

[21] T. Kawamura, K. Ouchi, and T. Nojiri. "Model and full scale CFD analysis of propeller boss cap fins (PBCF)". In: *Journal of Marine Science and Technology (Japan)* 17.4 (2012), pp. 469–480. ISSN: 09484280. DOI: 10.1007/s00773-012-0181-2.

[22] Y. Xiong, Z. Wang, and W. Qi. "Numerical study on the influence of boss cap fins on efficiency of controllable-pitch propeller". In: *Journal of Marine Science and Application* 12.1 (2013), pp. 13–20. ISSN: 16719433. DOI: 10.1007/s11804-013-1166-9.

[23] "Wartsila Energoprofin Brochure, https://www.wartsila.com/services/areas-of-expertise/services-catalogue/propulsion services/energoprofin". In: ().

[24] H. R. Hansen, T Dinham-Peren, and T Nojiri. "Model and Full Scale Evaluation of a 'Propeller Boss Cap Fins' Device Fitted to an Aframax Tanker". In: *Second International Symposium on Marine Propulsors, smp* 11.June (2011).

[25] K. W. Shin et al. "CFD-BASED OPTIMIZATION OF RUDDER BULB SYSTEMS". In: (2012), pp. 1–9.

[26] Y. Okada et al. "The development of " Ultimate Rudder " for EEDI". In: (2015).

[27] T. V. Terwisga and B. Schuling. "Lecture - Principles, desgin and glow analysis of ESDs - MARIN.pdf". In: (2019).

[28] G. M.E. E. Partnerships. *Propulsion Improving Devices*. URL: https://glomeep.imo.org/technology/propulsion-improving-devices-pids/ (visited on 01/16/2019).

[29] F. Mewis. "Three Years of Experience with the Mewis Duct ® - A Contribution to Ship Efficiency". In: ().

[30] K. Mizzi et al. "Design optimisation of Propeller Boss Cap Fins for enhanced propeller performance". In: *Applied Ocean Research* 62 (2017), pp. 210–222. ISSN: 01411187. DOI: 10.1016/j.apor.2016.12.006. URL: http://dx.doi.org/10.1016/j.apor.2016.12.006.

[31] H. K. Woud and D.Stapersma. *Propulsion and Electric Power Generation Systems*. ISBN: 1902536479.

[32] S.-k. Lee, Y.-f. Hsieh, and Z. Zhou. "Propeller Energy Loss Reutilization for Full Form Ship Propulsion". In: (2012).

[33] D. Hafermann and J. Marzi. "Propulsion Enhancements for a Greener Environment". In: *Second International Symposium on Marine Propulsors* June 2011.June (2011).

[34] S. C. Peter de Vos and K. Visser. "*Ship Resistance and Propulsion Model* - yet to be published". In: ().

Appendices

A Coefficients of ship resistance model

Nominal parameters		Coefficients				
$1000C_{E,nom}$	$v_{s,nom}$	a_{CE}	b_{CE}	c_{CE}	d_{CE}	k_{CE}
10.6863	15	0.333	10.2	0.07	-15	-0.06

Table 25: Coefficients of specific resistance[34]

Nominal parameters			Coefficients			
$K_{T,nom}$	$10K_{Q,nom}$	J_{nom}	a_{prop}	b_{prop}	c_{prop}	d_{prop}
0.1597	0.1942	0.4072	-1.0551	-0.8018	-0.1227	-0.1346

Table 26: Thrust and torque coefficients[34]

Nominal parameters		Coefficients	
w_{nom}	$v_{s,nom}$	c_w	d_w
0.2781	12.5	0.0880	0.1059

Table 27: Coefficients of wake fraction[34]

Nominal parameters		Coefficients	
w_{nom}	$v_{s,nom}$	c_w	d_w
0.2781	12.5	0.0880	0.1059

Table 28: Coefficients of wake fraction model[34]

Nominal parameters		Coefficients	
t_{nom}	$v_{s,nom}$	c_t	d_t
0.2009	12.5	0.0110	0.0147

Table 29: Coefficients of thrust deduction factor model[34]

Nominal parameters		Coefficients	
$\eta_{R,nom}$	$v_{s,nom}$	c_{η_R}	d_{η_R}
0.9808	12.5	0.0235	0.0279

Table 30: Coefficients of relative rotative efficiency model[34]

B Propeller losses of *Castillo De Tebra*

J	K_T	$10K_Q$	η_o	$\frac{K_T}{J^2}$ (c7)	η_a	η_r	η_f
0.1	0.275668	0.296793	0.147826	27.56668	0.1733	0.875	0.975
0.15	0.2583118	0.282122	0.218584	11.48052	0.2584	0.8775	0.964
0.2	0.2403658	0.266663	0.286919	6.009146	0.3398	0.89	0.949
0.25	0.221829	0.250416	0.352465	3.549264	0.41885	0.9	0.935
0.3	0.2027013	0.233381	0.414699	2.252237	0.49265	0.91	0.925
0.35	0.1829827	0.215557	0.472864	1.493736	0.5695	0.9175	0.905
0.4	0.1626732	0.196945	0.525837	1.016708	0.6352	0.925	0.895
0.45	0.141773	0.177545	0.571896	0.700113	0.6913	0.94	0.88
0.5	0.120282	0.1573565	0.608281	0.481126	0.7625	0.95	0.84
0.55	0.0981995	0.1363799	0.6302916	0.3246263	0.831	0.96	0.79
0.6	0.0755264	0.1146151	0.6292577	0.2097957	0.9029	0.968	0.72
0.65	0.0522625	0.0920620	0.5872772	0.1236983	0.92669	0.975	0.65
0.7	0.0284077	0.0687208	0.4605390	0.0579749	0.94189	0.978	0.5

Table 31: Propeller losses of *Castillo De Tebra*

C Ship data calculation

v_s (kn)	$1000C_E$	c1	P_E (kW)	R (kN)	$\frac{K_T}{J^2}$ (c7)	C_T
1	8.00164	5382.74616	0.73267	1.42431	0.68699	1.743493
2	7.78520	5237.14355	5.70279	5.54315	0.66416	1.677324
3	7.67896	5165.67747	18.98427	12.30189	0.65165	1.641489
4	7.61367	5121.75223	44.61711	21.68405	0.64342	1.619619
5	7.56422	5088.48676	86.57680	33.66128	0.63728	1.602803
6	7.52215	5060.18514	148.77263	48.20264	0.63248	1.589707
7	7.48585	5035.76705	235.10541	65.29255	0.62887	1.579069
8	7.45771	5016.83878	349.62541	84.95952	0.62662	1.573188
9	7.44449	5007.94628	496.92411	107.33630	0.62630	1.573188
10	7.46028	5018.56872	683.09759	132.79502	0.62911	1.580248
11	7.53317	5067.60293	918.08631	162.25193	0.63745	1.602803
12	7.71871	5192.41741	1221.28273	197.84907	0.65613	1.654993
13	8.12659	5466.79823	1634.80509	244.46780	0.69471	1.765674
14	8.97332	6036.39932	2254.57636	313.06603	0.77229	1.940473
15	10.68630	7188.72716	3302.39226	427.99278	0.92700	2.329079

Table 32: *Castillo De Tebra* data

v_s (kn)	w	t	η_H	η_R	J	K_T	$10K_Q$	η_o	$\frac{K_T}{J^2}$ (c7)	η_D
1	0.280512	0.201367	1.110003	0.982756	0.453	0.1405	0.176356	0.574388	0.684668	0.626578
2	0.278323	0.201127	1.106967	0.980747	0.4582	0.138289	0.174288	0.578622	0.658684	0.628184
3	0.276511	0.200926	1.104473	0.979089	0.4611	0.137053	0.173131	0.580936	0.644611	0.628211
4	0.275077	0.200763	1.102512	0.97778	0.4629	0.136285	0.172412	0.582355	0.636023	0.627787
5	0.274019	0.200637	1.101079	0.976822	0.4643	0.135687	0.171851	0.583449	0.629419	0.627533
6	0.273338	0.200549	1.100168	0.976214	0.4654	0.135217	0.171411	0.584303	0.624277	0.627541
7	0.273034	0.200499	1.099777	0.975956	0.4663	0.134832	0.17105	0.584998	0.620099	0.627898
8	0.273107	0.200487	1.099904	0.976049	0.4668	0.134618	0.17085	0.585382	0.61779	0.628443
9	0.273557	0.200513	1.10055	0.976492	0.4668	0.134618	0.17085	0.585382	0.61779	0.629097
10	0.274383	0.200576	1.101717	0.977285	0.4662	0.134874	0.17109	0.584921	0.620562	0.629779
11	0.275587	0.200677	1.103408	0.978428	0.4643	0.135687	0.171851	0.583449	0.629419	0.629895
12	0.277168	0.200816	1.105629	0.979922	0.46	0.137522	0.17357	0.580062	0.649914	0.628457
13	0.279126	0.200993	1.108386	0.981766	0.4513	0.141222	0.17703	0.57298	0.693379	0.623503
14	0.281461	0.201208	1.111689	0.98396	0.4386	0.14659	0.182037	0.562125	0.762022	0.614884
15	0.284173	0.20146	1.115548	0.986504	0.4141	0.156839	0.191554	0.539621	0.914627	0.593849

Table 33: *Castillo De Tebra*

v_s (kn)	J	n (rpm)	V_A $\frac{m}{s}$	T (kN)	Q (kNm)	P_D (kW)	P_S (kW)	$\frac{P_D}{P_S}$	η_{TRM}	P_B (kW)
1	0.453	11.40011	0.370105	1.777418	3.640028	1.169316	1.18268	0.9887	0.99	1.194626
2	0.4582	22.61004	0.742461	6.881528	14.47708	9.078221	9.181049	0.9888	0.99	9.273786
3	0.4611	33.78637	1.116488	15.22882	32.51989	30.2196	30.5588	0.9889	0.99	30.86748
4	0.4629	44.96232	1.491603	26.81882	57.80151	71.07047	71.86094	0.989	0.99	72.58681
5	0.4643	56.11521	1.867224	41.59045	90.28433	137.9637	139.4841	0.9891	0.99	140.893
6	0.4654	67.2421	2.242771	59.51241	129.9195	237.0725	239.6608	0.9892	0.99	242.0816
7	0.4663	78.33046	2.61766	80.52827	176.6103	374.4327	378.4442	0.9894	0.99	382.2668
8	0.4668	89.41567	2.991312	104.767	230.358	556.3362	562.2397	0.9895	0.99	567.9189
9	0.4668	100.5304	3.363143	132.4317	291.186	789.9004	798.2017	0.9896	0.99	806.2644
10	0.4662	111.7168	3.732571	163.8559	359.1761	1084.663	1095.951	0.9897	0.99	1107.021
11	0.4643	123.1867	4.099017	200.4288	435.0897	1457.524	1472.544	0.9898	0.99	1487.418
12	0.46	135.3457	4.461896	245.22	520.6914	1943.305	1963.133	0.9899	0.99	1982.962
13	0.4513	149.0463	4.820628	305.3785	619.898	2621.967	2648.452	0.99	0.99	2675.204
14	0.4386	164.6242	5.174632	386.7116	734.49	3666.667	3702.956	0.9902	0.99	3740.359
15	0.4141	186.1136	5.523324	528.8176	880.559	5560.998	5615.468	0.9903	0.99	5672.19

Table 34: *Castillo De Tebra*

D Model Implemented on *Castillo De Tebra*

D.1 Pre-swirl stator on *Castillo De Tebra*

RotL	$\frac{1-RotL}{100}$ (%)	f_{esd}	$\eta_{r_{pss}}$
0.0025	0.009975	0.009975	0.887475
0.0125	0.009875	0.01975	0.90975
0.01	0.0099	0.0297	0.9297
0.01	0.0099	0.0396	0.9496
0.0075	0.009925	0.049625	0.967125
0.0075	0.009925	0.05955	0.98455
0.015	0.00985	0.06895	1.00895
0.01	0.0099	0.0792	1.0292
0.01	0.0099	0.0891	1.0491
0.008	0.00992	0.0992	1.0672
0.007	0.00993	0.10923	1.08423
0.003	0.00997	0.11964	1.09764

Table 35: *Castillo De Tebra* - Decrease in rotational losses with a preswirl stator

FricL	$\frac{1-FricL}{100}$ (%)	f_{esd}	$\eta_{f_{pss}}$
-0.011	0.01011	-0.00169	0.962315
-0.015	0.01015	-0.00338	0.945617
-0.014	0.01014	-0.00507	0.92993
-0.01	0.0101	-0.00673	0.918267
-0.02	0.0102	-0.0085	0.8965
-0.01	0.0101	-0.0101	0.8849
-0.015	0.01015	-0.01184	0.868158
-0.04	0.0104	-0.01387	0.826133
-0.05	0.0105	-0.00175	0.78825
-0.07	0.0107	-0.01783	0.702167
-0.07	0.0107	-0.01962	0.630383
-0.15	0.0115	-0.023	0.477

Table 36: *Castillo De Tebra* - Increase in frictional losses with a preswirl stator

J	Rot gain (%)	Fric loss (%)
0.15	1	-0.16667
0.2	2	-0.33333
0.25	3	-0.5
0.3	4	-0.66667
0.35	5	-0.83333
0.4	6	-1
0.45	7	-1.16667
0.5	8	-1.33333
0.55	9	-0.16667
0.6	10	-1.66667
0.65	11	-1.83333
0.7	12	-2

Table 37: *Castillo De Tebra* - Applied gains

η_o	$\eta_{o_{pss}}$	η_{o_+}	η_{o_-}
0.147826	0.145724	0.151611	0.139953
0.218584	0.220681	0.229597	0.211942
0.286919	0.292321	0.304131	0.280745
0.352465	0.362119	0.376749	0.347779
0.414699	0.429584	0.446939	0.412572
0.472864	0.493772	0.513721	0.474219
0.525837	0.553404	0.575762	0.531489
0.571897	0.605529	0.629993	0.58155
0.608282	0.648321	0.674513	0.622647
0.630292	0.687198	0.714961	0.659985
0.629258	0.67659	0.703924	0.649797
0.587277	0.633375	0.658963	0.608293
0.460539	0.493149	0.513073	0.473621

Table 38: *Castillo De Tebra* - Gain in efficiency with a pre-swirl stator

D.2 Pre-duct on *Castillo De Tebra*

AxL	$\frac{1-AxL}{100}$ (%)	f_{esd}	$\eta_{r_{pd}}$
0.0851	0.009149	0.076577	0.334977
0.0814	0.009186	0.074407	0.414207
0.07905	0.00921	0.07211	0.49096
0.0738	0.009262	0.070021	0.562671
0.07685	0.009232	0.067298	0.636798
0.0657	0.009343	0.065588	0.700788
0.0561	0.009439	0.063713	0.755013
0.0712	0.009288	0.060186	0.822686
0.0685	0.009315	0.057846	0.888846
0.0719	0.009281	0.055129	0.958029
0.02379	0.009762	0.055351	0.982041
0.0152	0.009848	0.053179	0.995069

Table 39: *Castillo De Tebra* - Decrease in axial losses with a pre-duct

FricL	$\frac{1-FricL}{100}$ (%)	f_{esd}	$\eta_{f_{pd}}$
-0.011	0.01011	-0.00169	0.962315
-0.015	0.01015	-0.00338	0.945617
-0.014	0.01014	-0.00507	0.92993
-0.01	0.0101	-0.00673	0.918267
-0.02	0.0102	-0.0085	0.8965
-0.01	0.0101	-0.0101	0.8849
-0.015	0.01015	-0.01184	0.868158
-0.04	0.0104	-0.01387	0.826133
-0.05	0.0105	-0.00175	0.78825
-0.07	0.0107	-0.01783	0.702167
-0.07	0.0107	-0.01962	0.630383
-0.15	0.0115	-0.023	0.477

Table 40: *Castillo De Tebra* - Increase in frictional losses with a pre-duct

J	Axial gain (%)	Fric loss(%)
0.15	8.37	-0.16667
0.2	8.1	-0.33333
0.25	7.83	-0.5
0.3	7.56	-0.66667
0.35	7.29	-0.83333
0.4	7.02	-1
0.45	6.75	-1.16667
0.5	6.48	-1.33333
0.55	6.21	-0.16667
0.6	5.94	-1.66667
0.65	5.67	-1.83333
0.7	5.4	-2

Table 41: *Castillo De Tebra* - Applied gains

η_o	$\eta_{o_{pd}}$	η_{o_+}	η_{o_-}
0.147826	0.151358	0.157472	0.145364
0.218584	0.282865	0.294293	0.271664
0.286919	0.348596	0.362679	0.334791
0.352465	0.410903	0.427503	0.394631
0.414699	0.470180	0.489176	0.451561
0.472864	0.523791	0.544952	0.503049
0.525837	0.573618	0.596792	0.550902
0.571897	0.616143	0.641035	0.591744
0.608282	0.645666	0.671751	0.620098
0.630292	0.672608	0.699781	0.645972
0.629258	0.651170	0.677477	0.625384
0.587277	0.603586	0.627971	0.579684
0.460539	0.464206	0.482960	0.445823

Table 42: *Castillo De Tebra* - Gain in efficiency

D.3 Mewis duct on *Castillo De Tebra*

RotL	$\frac{1-RotL}{100}$	f_{esd}	$\eta_{r_{md}}$
0.0025	0.009975	0.005486	0.882986
0.0125	0.009875	0.010863	0.900863
0.01	0.0099	0.016335	0.916335
0.01	0.0099	0.02178	0.93178
0.0075	0.009925	0.027294	0.944794
0.0075	0.009925	0.032753	0.957753
0.015	0.00985	0.037923	0.977923
0.01	0.0099	0.04356	0.99356
0.01	0.0099	0.049005	1.009005
0.008	0.00992	0.05456	1.02256
0.007	0.00993	0.060077	1.035077
0.003	0.00997	0.065802	1.043802

Table 43: *Castillo De Tebra* - Decrease in rotational losses with a Mewis duct

AxL	$\frac{1-AxL}{100}$ (%)	f_{esd}	$\eta_{r_{md}}$
0.0851	0.009149	0.042543	0.300943
0.0814	0.009186	0.041337	0.381137
0.07905	0.00921	0.040061	0.458911
0.0738	0.009262	0.0389	0.53155
0.07685	0.009232	0.037388	0.606888
0.0657	0.009343	0.036438	0.671638
0.0561	0.009439	0.035396	0.726696
0.0712	0.009288	0.027864	0.790364
0.0685	0.009315	0.032137	0.863137
0.0719	0.009281	0.030627	0.933527
0.02379	0.009762	0.030751	0.957441
0.0152	0.009848	0.029544	0.971434

Table 44: *Castillo De Tebra* - Increase in axial losses with a Mewis duct

FricL	$\frac{1-FricL}{100}$ (%)	f_{esd}	$\eta_{f_{md}}$
-0.011	0.01011	-0.00169	0.962315
-0.015	0.01015	-0.00338	0.945617
-0.014	0.01014	-0.00507	0.92993
-0.01	0.0101	-0.00673	0.918267
-0.02	0.0102	-0.0085	0.8965
-0.01	0.0101	-0.0101	0.8849
-0.015	0.01015	-0.01184	0.868158
-0.04	0.0104	-0.01387	0.826133
-0.05	0.0105	-0.01575	0.77425
-0.07	0.0107	-0.01783	0.702167
-0.07	0.0107	-0.01962	0.630383
-0.15	0.0115	-0.023	0.477

Table 45: *Castillo De Tebra* - Increase in frictional losses with a Mewis duct

J	Rot. gain(%)	Fric loss(%)	Axial mult	Axial gain(%)
0.15	0.55	-0.16667	1.55	4.65
0.2	1.1	-0.33333	1.5	4.5
0.25	1.65	-0.5	1.45	4.35
0.3	2.2	-0.66667	1.4	4.2
0.35	2.75	-0.83333	1.35	4.05
0.4	3.3	-1	1.3	3.9
0.45	3.85	-1.16667	1.25	3.75
0.5	4.4	-1.33333	1.2	3
0.55	4.95	-1.5	1.15	3.45
0.6	5.5	-1.66667	1.1	3.3
0.65	6.05	-1.83333	1.05	3.15
0.7	6.6	-2	1	3

Table 46: *Castillo De Tebra* - Applied gains

η_o	$\eta_{o_{md}}$	η_{o_+}	η_{o_-}
0.147826	0.150493	0.159704	0.141642
0.218584	0.255714	0.271366	0.240676
0.286919	0.324679	0.344552	0.305586
0.352465	0.391051	0.414986	0.368054
0.414699	0.454806	0.482644	0.42806
0.472864	0.514038	0.545502	0.483809
0.525837	0.569223	0.604064	0.535748
0.571897	0.616959	0.654722	0.580677
0.608282	0.648741	0.688449	0.61059
0.630292	0.674302	0.715574	0.634647
0.629258	0.67028	0.711306	0.630862
0.587277	0.624725	0.662963	0.587986
0.460539	0.483671	0.513275	0.455227

Table 47: *Castillo De Tebra* - Gain in efficiency

E Power reduction with ESDs

v_s	n_e	P_B	$P_{B_{pss}}$	P_{B_+}	P_{B_-}
1	11.40011	1.194626	1.128862	1.089752	1.173464
2	22.61004	9.273786	8.754903	8.446831	9.102797
3	33.78637	30.86748	29.12291	28.09065	30.28417
4	44.96232	72.58681	68.45634	66.00509	71.2031
5	56.11521	140.893	132.8345	128.0574	138.163
6	67.2421	242.0816	228.1845	219.964	237.3538
7	78.33046	382.2668	360.268	347.2588	374.7468
8	89.41567	567.9189	535.209	515.8752	556.7561
9	100.5304	806.2644	759.8722	732.4487	790.433
10	111.7168	1107.021	1043.514	1005.915	1085.477
11	123.1867	1487.418	1402.644	1352.373	1458.702
12	135.3457	1982.962	1871.358	1805.162	1946.112
13	149.0463	2675.204	2528.165	2440.723	2628.411
14	164.6242	3740.359	3541.939	3422.533	3681.091

Table 48: Power reduction due to a Pre-swirl stator

v_s	n_e	P_B	$P_{B_{pd}}$	P_{B_+}	P_{B_-}
1	11.40011	1.194626	1.114154	1.079848	1.162709
2	22.61004	9.273786	8.657943	8.388449	9.035032
3	33.78637	30.86748	28.83167	27.92882	30.08682
4	44.96232	72.58681	67.81695	65.69109	70.77182
5	56.11521	140.893	131.6623	127.5218	137.4114
6	67.2421	242.0816	226.264	219.139	236.1363
7	78.33046	382.2668	357.3576	346.0572	372.9418
8	89.41567	567.9189	530.9872	514.2399	554.1627
9	100.5304	806.2644	753.8841	730.1291	786.7549
10	111.7168	1107.021	1035.069	1002.444	1080.095
11	123.1867	1487.418	1390.31	1346.735	1450.797
12	135.3457	1982.962	1851.886	1794.247	1932.532
13	149.0463	2675.204	2493.479	2416.677	2602.574
14	164.6242	3740.359	3475.909	3370.371	3629.391

Table 49: Power reduction due to a Pre-duct

v_s	n_e	P_B	$P_{B_{md}}$	P_{B_+}	P_{B_-}
1	11.40011	1.194626	1.116328	1.051629	1.180682
2	22.61004	9.273786	8.667707	8.165066	9.168698
3	33.78637	30.86748	28.85097	27.17728	30.52732
4	44.96232	72.58681	67.8431	63.90392	71.78637
5	56.11521	140.893	131.6838	124.0333	139.3607
6	67.2421	242.0816	226.2613	213.1136	239.4866
7	78.33046	382.2668	357.3028	336.5469	378.1713
8	89.41567	567.9189	530.864	500.0464	561.8395
9	100.5304	806.2644	753.7094	709.9953	797.6426
10	111.7168	1107.021	1034.927	974.9675	1095.196
11	123.1867	1487.418	1390.537	1310.016	1471.301
12	135.3457	1982.962	1853.451	1745.981	1960.81
13	149.0463	2675.204	2499.034	2353.592	2643.407
14	164.6242	3740.359	3490.739	3286.567	3692.32

Table 50: Power reduction due to a Mewis duct

F EEDI

v_s	n	EEDI	EEDI (Pre-swirl stator)	EEDI (Pre-duct)	EEDI (Mewis duct)
1	11.40011	10.3606	10.35789	10.35728	10.35737
2	22.61004	5.346895	5.336195	5.334196	5.334397
3	33.78637	3.861442	3.837459	3.833456	3.833721
4	44.96232	3.326213	3.283627	3.277035	3.277305
5	56.11521	3.224368	3.1579	3.148231	3.148409
6	67.2421	3.382485	3.286965	3.273764	3.273745
7	78.33046	3.725175	3.595569	3.578422	3.578099
8	89.41567	4.216577	4.047955	4.026191	4.025556
9	100.5304	4.840235	4.627653	4.600214	4.599413
10	111.7168	5.59655	5.33464	5.299813	5.29923
11	123.1867	6.513932	6.196103	6.149859	6.15071
12	135.3457	7.674148	7.290596	7.223677	7.229054
13	149.0463	9.279859	8.813403	8.703364	8.720987
14	164.6242	11.7547	11.1702	10.97569	11.01938

Table 51: Comparison of EEDI with the three ESDs

G Comparison of power savings by the ESDs

v_s	Pre-swirl stator	Pre-duct	Mewis duct
1	0.000658	0.000805	0.000783
2	0.005189	0.006158	0.006061
3	0.017446	0.020358	0.020165
4	0.041305	0.047699	0.047437
5	0.080586	0.092308	0.092092
6	0.138971	0.158176	0.158203
7	0.219989	0.249093	0.249641
8	0.327099	0.369317	0.370549
9	0.463922	0.523803	0.52555
10	0.635077	0.719527	0.720941
11	0.84774	0.971084	0.968814
12	1.116044	1.310761	1.295116
13	1.470383	1.81725	1.761699
14	1.984204	2.644505	2.496205

Table 52: Comparison of average power savings(%)

v_s	Pre-swirl stator	Pre-duct	Mewis duct
1	0.001049	0.001148	0.00143
2	0.00827	0.008853	0.011087
3	0.027768	0.029387	0.036902
4	0.065817	0.068957	0.086829
5	0.128357	0.133713	0.168597
6	0.221177	0.229426	0.28968
7	0.350081	0.362097	0.457199
8	0.520437	0.536789	0.678725
9	0.738157	0.761353	0.962691
10	1.011061	1.045773	1.320539
11	1.350452	1.406826	1.774017
12	1.778	1.887158	2.369809
13	2.344804	2.585268	3.216118
14	3.178266	3.699883	4.537919

Table 53: Comparison of average power savings(%) $\longrightarrow$ +2% deviation from average savings

v_s	Pre-swirl stator	Pre-duct	Mewis duct
1	0.000212	0.000319	0.000139
2	0.00171	0.002388	0.001051
3	0.005833	0.007807	0.003402
4	0.013837	0.01815	0.008004
5	0.027301	0.034816	0.015323
6	0.047279	0.059454	0.025951
7	0.0752	0.093251	0.040955
8	0.111627	0.137561	0.060793
9	0.158313	0.195095	0.086218
10	0.215448	0.269261	0.118253
11	0.287158	0.366215	0.161169
12	0.368502	0.504307	0.221523
13	0.467926	0.726296	0.31797
14	0.592677	1.109681	0.480392

Table 54: Comparison of average power savings(%) $\longrightarrow$ -2% deviation from average savings